PION PRODUCTION IN NUCLEUS-NUCLEUS COLLISIONS BELOW A FEW GeV/NUCLEON - PAST, PRESENT AND FUTURE*

L. S. Schroeder

Lawrence Berkeley Laboratory
Berkeley, California 94720
University of California

ABSTRACT

A general review of experimental data on pion production in A-A collisions for incident energies below a few GeV/nucleon is presented. Early data on inclusive pion spectra which served as the genesis for present pion measurements are discussed. The majority of the paper will be devoted to present pion experiments, with an emphasis being placed on what such experiments tell us about the general features of high energy A-A collisions. Particular attention will be given to multi-pion production as studied in recent streamer chamber experiments. The review ends with projections on future experiments with the heavier beams that will be available in 1982 at Berkeley, and the higher energy beams that will hopefully be available in the not too distant future.

---

*This work is supported by the Nuclear Physics Division of the U.S. Department of Energy under Contract No. W-7405-ENG-48.
**This manuscript was printed with figures provided by the author.

INTRODUCTION

We have had almost one decade of research on high energy nuclear collisions using projectiles heavier than a proton. For incident energies above 1 GeV/nucleon, data has been obtained from the Synchophastron at Dubna, Saturne I and its successor Saturne II at Saclay, the Penn-Princeton Accelerator (now closed) and the Bevatron/Bevalac in Berkeley, and recently the ISR at CERN. Although the data came in very slowly at first, we are now at a point where experimental and theoretical papers on such collisions are quite substantial and are attracting considerable interest. Thus, it would be useful to pause and catch our breathe, and see how far we have come in understanding high energy nucleus-nucleus (A-A) collisions.

My intention is to review what we know about high energy A-A collisions as viewed through the microscope of pion production. Pions are particularly interesting from the point-of-view that they must be created in the collision process and not merely liberated as in the case of nucleons. As such, they potentially reflect direct information on the basic dynamics of the collision process. It is this type of information that we need, to ascertain whether there are new and unusual states of nuclear matter being created in high energy nuclear collisions. However, we also need to remember that there are less exotic, but equally interesting, questions that can be addressed by observations of pions from such collisions.

I will restrict my attention to pion production in the collision of projectiles ranging from protons to the heaviest presently available (typically mass ~40), at beam energies up to a few GeV/nucleon. Before proceeding further, it is instructive to point out some of the characteristic features

of N-N collisions in this energy range, as the N-N interaction will serve as a useful base-line for comparing the results from high energy A-A studies. In Fig. 1(a)[1] is displayed the elastic and total cross sections for p-p collisions as a function of beam momentum. $\sigma_T(pp)$ is observed to fall rapidly with beam momentum until the threshold for pion production ($NN \rightarrow NN\pi$) is reached at about 800 MeV/c; after which $\sigma_T(pp)$ rises and flattens out at about 42-44 mb for momenta above a few GeV/c. The majority of this increased cross-section is due to pion production, with the production of strange particles accounting for a few percent. Figure 1(b) shows a blow-up of these trends for beam momenta up to 5.5 GeV/c, with the thresholds for various channels being indicated. Clearly, in the energy range of interest for this paper, pion production accounts for a very sizable part of the total p-p cross-section.

Figure 2[1] serves to demonstrate that over this energy range we are primarily concerned with $NN \rightarrow NN\pi$ and $NN\pi\pi$; with single pion production accounting for well over one-half of the total yield of pions. Closer examination of these trends show that a majority of the single pion production arises from a simple 2-body process involving the 33-resonance; namely, $NN \rightarrow N(\Delta) \rightarrow N(N\pi)$. In Fig. 3(a)[2] we see the Q-value distribution ($Q = M(\pi N) - (M_\pi + M_n)$) for the πN system produced in the reactions, $pp \rightarrow pp\pi^0$ and $pn\pi^+$, using 970 MeV protons. The broad peak in the distribution shows the strong influence of the $\Delta(1232)$ in this reaction, with the solid curve representing the predictions of phase space. Figure 3(b)[3] shows the $p\pi^+$ effective mass distribution for the reaction $pp \rightarrow pn\pi^+$ at a higher bombarding energy of 4.64 GeV. The production of the $\Delta^{++}(1232)$ still dominates the reaction, with some

evidence for the production of higher lying resonances near 1920 and 2360 MeV. Clearly, we see that the production of pions in N–N collisions at energies $\lesssim$ 4–5 GeV is primarily through the production of a nucleon excited state and its subsequent decay to $N\pi$ or possibly $N\pi\pi$.

In an A–A collision, a pion once produced in the nuclear media, must make its way through the residual matter on its flight to the detector. Figure 4[4] shows a representation of the total cross-sections for $\pi^+ p$ and $\pi^- p$ interactions as a function of pion momentum. The strong resonances in the πN system are clearly demonstrated for pion momenta below ~2 GeV/c. Above ~2 GeV/c, $\sigma_T(\pi^{\pm} p)$ levels off. This indicates we must be careful to take into account the possible effects of absorption, charge exchange, etc., on measured pion spectra.

This review will proceed in three steps:

(1) PAST: A brief survey of the results of earlier work on pion production and its motivation. In general, these experiments served as guides for the present generation of experiments.

(2) PRESENT: A more thorough discussion of recent pion results in A–A collisions and the general picture that unfolds. Whereas, the earliest experiments were predominately single-particle inclusive studies, the present trend is to more exclusive measurements such as $\pi\pi$ correlations, correlations with multiplicity, etc. Emphasis will be placed on recent streamer chamber results where we start to look at the trends on an event-by-event basis, rather than trends integrated over many events.

(3) FUTURE: Finally, I will discuss some of the physics that can be studied through pion production measurements with the heavier beams that are expected at Berkeley in the next year or so. In addition, I will speculate about possibilities with very high energy nuclear beams which are being proposed for future accelerators.[5]

PAST EXPERIMENTS ON PION PRODUCTION

In this section we consider some of the early work on pion production, restricting our attention to:

(1) Single-particle inclusive experiments of the form, $A+B \rightarrow \pi^{\pm}+X$, and

(2) Pion multiplicity studies with a streamer chamber.

1) Single-Particle Studies

Experiments on inclusive pion spectra were some of the first studies in high energy A-A collisions. Beyond their simple survey nature, a prime factor motivating these experiments was the search for pions with energies far beyond those that could be achieved in simple free N-N collisions. The observation of such pions might then indicate the presense of cooperative phenomena in these collisions. Early work done at Dubna[6] involved the study of forward high energy π^- production by proton and deuteron beams of the same kinetic energy. They found that the ratio:

$$R = \frac{\sigma(d + Cu \rightarrow \pi^- + x)}{\sigma(p + Cu \rightarrow \pi^- + x)}$$

for equal kinetic energy (~4 GeV/nucleon) beams was approximately a constant for pions produced near the kinematic limit. They claimed that these results indicated that the deuteron interacted as a single particle, in the interaction.

Papp et al.[7] studied forward (fixed LAB angle = 2.5°) pion production in the following reactions:

$$\begin{pmatrix} p \\ d \\ \alpha \\ C \end{pmatrix} + A \rightarrow \pi^{\pm}\ (2.5^{\circ}) + x,$$

with 1.05–4.2 GeV protons, 1.05 and 2.1 GeV/nucleon α's, and 1.05 GeV/nucleon carbon nuclei. An interesting feature of these studies was the observation that the forward pion spectra were observed to scale at incident energies as low as ~1 GeV. Figure 5(a) shows the results for π^- production by 1.05–4.2 GeV protons on a carbon target. Plotted is the invariant cross-section $[(E/k^2)(d^2\sigma/d\Omega dk)]$ vs. the scaling parameter, $x' = (k^*_{11}/k^*_{11\ max})$. A similar plot for 1.05 and 2.1 GeV/nucleon deuterons and alphas is shown in Fig. 5(b). In both cases, the data are seen to lie on a universal curve, suggesting the premature scaling of negative pions at energies as low as ~1 GeV. Schmidt and Blankenbecler, using a hard-scattering model[8], predicted that the pion cross-sections should be of the form, $(1-x')^N$, where the value of N is determined from simple counting arguments. Figure 6(a,b) agains shows the data, where the solid curves are the predictions of their model which are seen to be in good agreement with the data. Their model assumes that the proton interacts collectively with the whole nucleus, a condition necessarily satisfied only near x' = 1. Why it fits so well over the whole range of x' from ~0.2 to 1.0 was something of a mystery. We will return to this question later in our discussion of recent results on pion production at 180°.

The early experimental data from both Dubna[6] and Berkeley[7] indicated that nuclear projectiles do create pions with energies considerably larger than could be obtained from either N–N or N–A collision at the same kinetic

energy/nucleon of the projectile. The question remained as to whether these high energy pions were the result of several nucleons of the projectile acting in a collective fashion, or just a single N-A collisions with the inclusion of Fermi motion in both target and projectile. Figure 7 shows the results of a calculation by the Berkeley group[7] based on a model in which all pions are produced in individual nucleon-nucleus collision with Fermi motion included. The form of the single pion production cross-section in this model is:

$$\sigma_{aA}^{\pi}(\vec{p}_a, \vec{k}_\pi) = \sum_{N}^{a} W_{aN}(\vec{p}_a, \vec{p}_N)\, \sigma_{NA}^{\pi}(\vec{p}_N, \vec{k}_\pi)\, d^3p_N,$$

where W_{aN} = momentum distribution of the nucleon in the projectile appropriately transformed to the laboratory frame, σ_{NA}^{π} are measured nucleon-nucleus pion production cross sections (which thereby fold in the Fermi motion associated with the target). The model assumed charge symmetry ($\sigma_{pC}^{\pi^+} = \sigma_{nC}^{\pi^-}$) to obtain neutron-induced cross-sections from carbon. Since the production was at a fixed laboratory angle, the measured cross-sections were folded with $\exp[-5\, k_\pi \sin(\theta_{k\pi} - \theta_{pN})]$. The predictions of the model are in reasonable agreement with the data, except for the 2.1 GeV/nucleon alpha induced results where the model seriously underestimates the yield. The momentum distribution for nucleons inside the alpha particle were taken from elastic electron scattering information, where it is known that high relative momentum components do not contribute. These components could be very important in producing high energy pions with alpha particles. Thus, the results of this model appear to support an independent particle approach,

whereas the Dubna group[6] claims that their results were indicative of collective effects. It needs to be pointed out that for the case of production by deuterons, one cannot distinguish between a Fermi motion model and a model with collective effects, since they amount to the same thing, i.e., for the deuteron case, large Fermi momentum components necessarily imply that the two nucleons are spatially close together and are, therefore, correlated.

Additional insight into the production mechanism for pions can be obtained by studying the dependence of the cross-section on the target mass. The pion production cross-sections were parameterized in the form[7]: $\sigma \propto A^n$, where A is the mass of the target. A plot of the exponent n as a function of pion laboratory momentum for 2.1 GeV/nucleon alphas is shown in Fig. 8. For momenta $\geq$1 GeV/c the dependence of $A^{1/3}$ suggests peripheral production. For pions with momenta <1 GeV/c, the dependence is more pronounced, suggesting that these pions are produced in more central collisions. Similar features are observed in the proton and deuteron induced data.

Finally, before leaving forward pion production, we note that in one of the closing experiments of the Penn-Princeton accelerator, $\pi^{\pm}$ spectra from 100–700 MeV were obtained for ^{14}N nuclei incident at 520 MeV/nucleon on a variety of targets.[9] The pions were found to be produced with an $A^{1/3}$ dependence on the target mass, as expected if the interaction occurs on the nuclear surface (peripheral). The data were compared to a model involving pions produced in single nucleon-nucleus collisions with Fermi motion folded in. None of their assumptions about single-nucleon momentum distributions were able to fit the data for pions with $T_\pi \geq 415$ MeV, possibly indicating some more exotic mechanism at work.

As a follow-up to the work on forward pion production at Dubna, measurements[10,11] of the reaction, $p+A \rightarrow \pi^{\pm}(180^{\circ})+x$, were undertaken. A principal reason for studying production of energetic pions from nuclei in the backward direction is that in free N-N collisions such production is kinematically restricted. Observation of pions beyond this kinematic limit may then be evidence for exotic production mechanisms such as production from clusters. In these experiments[10] using 5.14 and 7.52 GeV protons they observed charged pions at 180° with energies up to four times larger than expected for free N-N collisions. They claimed that simple Fermi motion could not account for this effect and suggested that the dominant mechanism was an interaction between the incident proton and multi-nucleon clusters in the target nucleus, referring to this mechanism as cumulative production. A variety of models involving clusters[12-15] in one form or another have been invoked to explain these results.

Figure 9(a) shows their pion cross-sections plotted against the kinetic energy of the pion. The spectra are seen to be exponential, with a slope parameter, $T_0 \sim 60$ MeV, found to be independent of bombarding energy. An experiment with 28.5 GeV protons[16] studying backward pion production also observed a slope consistent with the lower energy results from Dubna. This suggests that a limiting value has been reached. Does it persist to energies lower than ~5 GeV and where does it start to break down? Questions such as this stimulated second generation experiments which will be described in the next section. Finally, as shown in Fig. 9(b), they found that the A-dependence of charged pions produced at 180° increased from a value of about $A^{2/3}$ for pions with energies below that expected for free N-N production (typically

~250 MeV), then increases and appears to flatten out at $A^{1.0-1.2}$ for large pion energies. This is reminescent of the A-dependence seen at large $p_\perp$ in FNAL energies.[17] There is, however, a difference we must keep in mind; namely the 180° production experiments are done at $p_\perp = 0$, which is suggestive of softer peripheral collisions. The physics, possibly via hard-scattering mechanisms, is probably different for large $p_\perp$ phenomena.

2) Streamer Chamber Results

We now turn from the single particle inclusive experiments, to those which can provide considerably more information on particles resulting from a nuclear collision. These experiments utilize the streamer chamber, a visible detector[18] for studying particle interactions. Streamer chambers have the following favorable characteristics:

(a) Detection of charged particles over 4π.

(b) Good efficiency for registering large numbers of charged particles. An example of this is shown in Fig. 10, where a 1.8 GeV/n ^{40}Ar projectile interacts with a Pb nucleus, to produce ~80 charged particles in the final state. The tracks curving counter-clockwise in the magnetic field surrounding the chamber are negative pions.

(c) The device can be selectively triggered; this means that one can obtain a large sample of events of a particular type such as central or high $p_\perp$ collisions.

A UC Riverside/LBL collaboration[19] investigated negative pion production by 0.4-2.1 GeV/nucleon ^{12}C and ^{40}Ar beams from a variety of targets. The multiplicity distributions for negative pions are shown in Fig. 11 for both a light (LiH) and heavy (Pb_3O_4) target. For the case of 1.8 GeV/nucleon

$^{40}Ar+Pb_3O_4$ collisions, up to 14 π^-'s were observed. Remember that on the average one expects approximately equal numbers of π^+, π^-, π°. Thus, large numbers of pions are produced in these nuclear collisions. The turn over for small n_{π^-} in these distributions is due to an ~10-15 percent inefficiency introduced by the experimental trigger used to take the pictures.[19]

A number of models which employ differing assumptions have been applied to these data. In Fig. 12 are shown the predictions of two such calculations[20,21] compared to the 1.8 GeV/nucleon $Ar+Pb_3O_4$ multiplicity distributions. The diamond-shaped points in Fig. 12(a) are the result of a multiple-collision model[20] based on using nucleon-nucleon data for pion production (pion absorption neglected), nuclear density distributions, and the assumption of straight-line trajectories. The calculation is seen to disagree with the data, particularly for large multiplicities. The inclusion of intermediate baryon resonances does reduce the high multiplicity end somewhat, but not enough for agreement. It was concluded, that the high multiplicity end might be sensitive to coherent production mechanisms.

Somewhat at the opposite extreme of the independent nucleon-nucleon collision model just described, is a thermal model calculation,[21] in which the fireball model[22] was used to calculate the pion yields. In this model, pions are assumed to come to chemical and thermal equilibrium during the collision process. On expanding, the various components of the fireball created in the collision established their asymptotic state (no additional production or absorption) at a critical "freeze-out" density ρ_c. Usually, $\rho_c = (1/4\text{-}1/2)\ \rho_0$, with $\rho_0 = 0.17\ fm^{-3}$. The solid lines in Fig. 12(a) are the results of this calculation, the two lines differing in the choice of

impact parameters used. Agreement with the data is evident. An interesting result of this calculation is indicated by Fig. 12(b). The larger the π^- multiplicity, the smaller the impact parameter b. Thus, a way of selecting small impact parameters, and therefore obtaining central collision events, appears to be by selecting high multiplicities. It is of course, in the central collisions of nuclei, that we hope to best create the conditions of high temperatures and densities that could lead to new and unusual states of nuclear matter. This theme of multiplicities as a selector of impact parameters has been used by several groups for second generation experiments that will be described shortly.

Figure 13 shows the predictions of the collective tube model[23] (CTM) compared to the streamer chamber data. This model has been extensively used to predict results for high energy hadron-nucleus collisions.[24] In applying the CTM to nucleus-nucleus collisions, they assumed that the primary interaction occurs between a tube of nucleons in the projectile and a tube of nucleons in the target. In the c.m. system the colliding tubes are Lorentz contracted. The CTM then assumes that the tube-tube collisions resemble elementary particle-particle collisions, where appropriate averaging over impact parameters and nuclear shapes must be considered. The results are in remarkable agreement with the data. How this arises is unclear, since the CTM was originally applied to data at much higher energies. It should be remembered that at the highest Bevalac energies, the c.m. energy/nucleon is only ~400 MeV! The authors conclude that the agreement between the CTM predictions and the multiplicity data, even at the lowest Bevalac energies, is not accidental. Their calculations are also found to be in agreement with

17.8 GeV/c α-nucleus π^- multiplicity distributions obtained in early streamer chamber studies at Dubna,[25] and are shown in Fig. 14.

Before leaving the discussion of streamer chamber results it is worth noting some of the other trends exhibited by the data. From Bevalac results:

(a) The $p_\perp$ distribution of the produced pions is independent of pion multiplicity.

(b) The momentum and energy distributions are independent of pion multiplicity.

(c) The pion multiplicity appears to be ∝ total charged particle multiplicity, but with the proportionality depending on the bombarding energy, and

(d) If the data are plotted as shown in Fig. 15, $\langle N_{\pi^-}\rangle \sigma_{N_{\pi^-}}/\sigma_{inel}$ vs. $N_{\pi^-}/\langle N_{\pi^-}\rangle$, the distributions are found to be ~ independent of target/projectile combination, except for those at the lowest bombarding energies.

The Dubna streamer chamber studies found that they could relate the pion multiplicity distribution observed for α-particles to that produced by high energy protons when they choose the proton beam energy to correspond to the energy where $\langle n_- \rangle_{pp} = \langle n_- \rangle_{\alpha A}$.

SUMMARY OF PAST WORK

Some of the highlights of the early studies of pion production in A-A collisions include:

(A) Pions at both forward and backward angles were found to be produced with energies considerably larger than those expected from simple free N-N collisions. Possible mechanisms for such energetic pions might be internal nucleon motion inside target and projectile or collective effects such as nucleon clusters. It is not clear that these are necessarily different effects, or merely different words for the same effect.

(B) More exclusive studies using streamer chambers indicated many trends which were weakly dependent on the target/projectile combination used. A wide variety of models have been compared to the data, with the most notably failure being the single N-N collision model, although the neglect of pion absorption could play a role in this. The remaining models (thermal and CTM) had excellent agreement with the multiplicity data. However, comparison with detailed angular and momentum distributions need to be done to see if these models continue to hold up. It became clear that impact parameter selection via multiplicity could be a very fruitful tool for later experiments.

(C) Although no prominent feature indicative of new states of nuclear matter (such as pion condensates, abnormal matter or density isomers) were manifested in these early pion production results, it is apparent that there are many features not explainable by simple N-N collision arguments.

PRESENT RESULTS FROM PION PRODUCTION STUDIES

I now want to focus attention on the large bulk of new data presently being published on pion production in A–A collisions. By present experiments, I loosely mean those which were taking data during the period of approximately 1976–79, and have either published results or are close to doing so. This covers a period of immense activity in the field, where second generation experiments were started and completely new areas of studies with pions in A–A collisions were undertaken.

The material that I intend to cover is listed below:

(1) 2nd generation single-particle inclusive studies, including some with associated multiplicity information. Here I will discuss such features as:

   (A) high energy charged pion production in the mid-rapidity region

   (B) low energy charged pion production (typically $T_{\pi}^{LAB} < 100$ MeV)

   (C) energy dependence of neutral pion production

   (D) charged pion production at 180° as a function of projectile target and bombarding energy; and production to the kinematic limit at 0°.

(2) Latest streamer chamber results, including negative pion excitation function for central collisions of the Ar+KCl system from 0.4–1.8 GeV/nucleon and Hanbury-Brown/Twiss analysis.

1) Single Particle Inclusive Results + Much More

A) Charged Pion Production in the Mid-Rapidity Region

The early results as we have seen were restricted to the extreme forward and backward region, that is for small values of $p_\perp$. To obtain a more comprehensive view of the mechanisms responsible for pion production in A-A collisions, one also requires information on the transverse yields of pions. Whereas forward-backward production appears to be dominated by peripheral collisions, production at wide angles is most likely populated by more central collisions. Therefore, wide angle production might reveal, in a cleaner fashion, the presence of exotic production mechanisms.

Using a single-arm spectrometer with associated multiplicity capability, Tanihata et al.[26] have measured both π^+ and π^- production for pions with $80 < T_\pi < 1000$ MeV over the angular range $150^\circ < \theta_{LAB} < 45^\circ$. These measurements have been carried out at 0.4, 0.8 and 2.1 GeV/nucleon, using projectiles ranging from p to ^{40}Ar. Figure 16 shows their results for an 0.8 GeV/nucleon Ar colliding with KCl and Pb targets (KCl is often used as a target with approximately the same mass as ^{40}Ar). The data are displayed in the nucleon-nucleon c.m. frame, although this is not the best choice for the Pb target. The lines are contours of constant invariant cross-section in the $p_\perp$ and $p_\parallel^*$ planes. An isotropic distribution in the nucleon-nucleon c.m. would yield a semi-circle in this plot. For pions with $p^\pi_{c.m.} > 200$ MeV/c, the shapes of these contours are almost independent of the target and centered on $p_\perp^* = p_\parallel = 0$. For lower momentum pions, the contours are shifted towards the target frame for the case of Ar+Pb. Also, the contours for the lower energy pions are seen to be flatter than those at high energies. This

suggests that there might be different production mechanisms producing high and low energy pions, with the high energy pions being qualitatively consistent with the expectations of simple nucleon-nucleon processes. For low energy pions, shadowing effects of projectile and target matters could be important.

Pion energy distributions are shown in Fig. 17, and are seen to be approximately exponential in shape. Two theoretical calculations, those of the firestreak[27] and a hard-scattering model,[28] are compared with the ^{20}Ne+NaF data. The firestreak model overestimates the pion yield, typically by a factor of 2 or larger. This overestimate also occurs when the thermal model is compared with other data. The hard-scattering model, which assumes only a single hard-scattering and uses a nucleon momentum distribution extracted from backward proton production measurements,[29] is in better agreement. However, it does not predict the continuing rise of the cross-section for low pion energies. The model is also not able to reproduce trends associated with the angular distributions of the pions.

Additional trends are available from these data. Both pions and protons released in these collisions are found to have invariant cross-sections which can over a wide range of particle energy be parameterized as $\sigma_{inv} \propto e^{-E/E_o}$, where E is the kinetic energy of the particle measured in the nucleon-nucleon c.m. Figure 18 shows the dependence of the slope parameter E_o on bombarding energy. A number of features can be noted:

(1) $E_o(p) > E_o(\pi)$.

(2) The pions clearly cool down the system, otherwise one would expect $E_o(p)$ to rise linearly with E^* (beam energy/nucleon).

(3) Although the trends of the thermal [27] and hard-scattering model [28] rise with c.m. energy, neither provides an adequate representation of the data.

Noting the differences between the value of E_o for protons and pions, Siemens and Rasmussen [30] suggested that the thermal model should be modified by including effects due to expansion of the system (blast wave of nucleons and pions). In this approach, the available energy is shared between translational energy of the blast, and thermal motion of the particles in the fireball. The model is able to qualitatively explain the differences in E_o for pions and protons, but is unable to predict either absolute cross-sections or observed angular distributions.

Figure 19 shows the integrated yield ($d\sigma/d\Omega$) at $\theta_{c.m.} = 90^\circ$ for negative pions and protons as a function of the c.m. beam energy. The models have been arbitarily normalized to the proton yield at the lowest bombarding energy. Since, in a thermal model the yield of protons is solely determined by the number of participant nucleons, one expects an independence with bombarding energy. The hard-scattering model on the other hand must reflect the effects of nucleon-nucleon scattering, so that as the energy increases we expect fewer protons at wide angles. The negative pion yields exhibit a threshold-like behavior as expected, rising rapidly with energy. Both models are able to reproduce this trend (again remember the arbitary normalization mentioned above).

B) Low Energy Pion Production

In all previous discussions I have been concentrating on pions with energies >100 MeV. Now I want to consider results from two experiments which measured production of positive pions with energies $20 < T_\pi < 100$–125 MeV. These experiments involved use of range-energy telescopes and the $\pi^+ \rightarrow \mu^+$ decay for particle identification. In general, one hopes that lower energy pions will contain vital information concerning the early stage of the collision process. Their ability to do this resides in the fact that, as seen in Fig. 4, the πN cross-section falls off rapidly below the $\Delta(1232)$ resonance. For energies below 100 MeV, the mean free path of pions in nuclei becomes longer than typical nuclear sizes. Higher energy pions can of course become degraded through nuclear interactions as they exit the interaction volume, producing a component in the low energy spectrum.

To see the transition from high to low energy pions, the results of experiments with overlapping data are shown in Fig. 20. The pion cross-section is observed to roll over as $T_\pi \rightarrow o$, rather than continuing to increase exponentially. This roll over is partially due to Coulomb effects, although the $\Delta(1232)$ probably also plays a role.

As previously stated, a central theme of high energy A-A central collisions is the search for new phenomena. Along this line are recent observations of an enhancement in the π^+ spectrum at mid-rapidity ($\theta_{c.m.} = 90^\circ$).[31,32] Chiba et al.[31] studied the reaction, $Ne+NaF \rightarrow \pi^+ + x$ at 800 MeV/nucleon. Results of this experiment are shown in Fig. 21 and compared with $p+p \rightarrow \pi^+ + x$ data. The solid lines are contours of constant cross-sections and are seen to produce a broad bump near $\theta_{c.m.} = 90^\circ$ for the Ne+NaF case, and no bump

for the p+p results. A similar effect is not observed in their 400 MeV/nucleon data. Wolf et al.[32] have studied $Ar+^{40}Ca \rightarrow \pi^+ + x$ at 1.05 GeV/nucleon, with the added feature of multiplicity selection to differentiate between peripheral and central collisions. Their results, which are found to be insensitive to multiplicity selection, are shown in Fig. 22 together with $p+p \rightarrow \pi^+$ data. Again, a broad peak appears centered around mid-rapidity and $p_\perp / m_\pi c \sim 0.5$. They find that a cascade mechanism does not reproduce this effect. Recently, Libbrecht and Koonin[33] have performed calculations which indicate that the peak in the π^+ spectrum could be due to a Coulomb focussing effect. That is, the Coulomb field tends to repel π^+'s produced as angles away from 90°, causing them to be deflected into the region around $\theta_{c.m.} = 90°$. Figure 23 shows results of their calculations with differing assumptions on the charge density associated with the positive matter repelling the outgoing π^+. Such a model would predict a suppression for π^-'s in the same region. Experiments to measure π^-'s in the mid-rapidity region have been completed and results are expected within the next few months.[34] If the various interpretations such as cascade, Coulomb or $\Delta(1232)$ effects, do not explain this mid-rapidity behavior, more exotic mechanisms will have to be seriously considered.

Recently, low energy π^+ and π^- production at 0° has been measured for energies spanning the range 125–400 MeV/nucleon.[35] The initial intention of the group[35] was to study low energy pions produced both above and well below the free N-N threshold (about 270 MeV). Being below threshold such measurements provide data for testing Fermi motion calculations or possibly yield information on cooperative nuclear processes (exotic or otherwise). A

striking feature of the data of Benenson et al.[35] is the unexpectedly large π^-/π^+ ratio for pions with velocities near the projectile velocity. This is shown in Fig. 24 for the Ne+NaF results. The peak, which is most clearly seen in their 400 MeV/nucleon data, can be qualitatively understood in terms of the Coulomb distortion of pion wave functions near the projectile charge. Thus, there appears to be a possibility of producing pionic-like atoms in A-A collisions. Turning to the energy dependence, Fig. 25 demonstrates the rapid decrease of pion yield with decreasing bombarding energy. The data have been compared with a thermal model[22] and a one-collision Fermi-gas model[36] (with inclusion of the $\Delta(1232)$). Only at the lowest bombarding energy does the one-collision model agree to within a factor of 2 of the data. This gives weight to the idea that several different production mechanisms appear to be involved throughout this energy region.

C) Neutral pion Production

DeJarnette et al.[37] have measured high energy (>50 MeV) gamma-ray production in ^{12}C+Pb collisions from 1.05-2.1 GeV/nucleon. The high energy gammas result from the decay, $\pi^\circ \rightarrow \gamma\gamma$. By measuring an excitation function, they can look for structure which might indicate the presence of unusual states of nuclear matter. Their experiment concentrated on production at wide angles, and had a variety of detectors which could be used to make multiplicity cuts on the data. Figure 26 shows the results of several different selections of the data. None of the curves exhibit any departure from a smooth transition with energy. The yield of high energy gamma rays was found to increase by a factor of two over this energy range (recent streamer chamber results[49] agree with this). Selecting on multiplicity

indicated that there were more high energy gamma rays (and fast charged pions) produced in high multiplicity events than in low multiplicity events.

D) Production at 0° and 180° Beyond Simple N-N Kinematic Limits

One of the areas of pion production measurements that has been heavily influenced by first-generation experiments is that of high energy pions produced beyond the kinematic limits of free N-N collisions. I now turn to a discussion of this topic, one which is near to my heart.

Using the CERN synchrocyclotron, Aslanides et al.[38] have studied the inclusive process, $^{3}He+^{6}Li \rightarrow \pi^{-}+x$ at 910 MeV, up to the kinematic limit for the coherent reaction ($^{3}He+^{6}Li \rightarrow +^{9}C+\pi$). Figure 27 shows the inclusive pion spectrum. The region near the end point of this spectrum is shown in the insert. They claim that the change in shape near the end point is due to the coherent reaction, but finite resolution and low statistics do not allow a distinct bump to show up. They have attempted an analysis of the inclusive pion spectrum in terms of the elementary process, $NN \rightarrow NN\pi$. Use of conventional nucleon momentum distributions do not provide a reasonable fit to their spectrum, again suggesting the need for collective mechanisms or larger high-momentum components. In terms of the Feynman scaling parameter, their data can be parameterized as $(1-x')^{N}$, with N = 9 up to x' = 0.7. For larger value of x', the value of N decreases, being ~4 for $0.9 < x' < 1.0$. It is actually near x' ~ 1 that the assumptions of the Schmidt and Blankenbecker model[8] (see earlier discussion) should be valid.

I now turn to the results from our recent measurements of pion production at 180° in A-A collisions. We have measured the following:

$$A_1 + A_2 \rightarrow \pi^{\pm}(180^{\circ}) + x,$$

where A_1 = p,α,C,Ar and A_2 = C,Al,Cu,Sn,Pb. Incident energies were 0.8–4.89 GeV for protons, 1.05 and 2.1 GeV/nucleon for alphas and carbon, and 1.05 and 1.8 GeV/nucleon for Ar.

First, I will consider results on $\pi^{\pm}$ production by protons.[39] Our motivation was to follow-up the study of pion production well beyond the free N-N kinematic limit. The backward direction also has the advantage that far fewer processes contribute and therefore a clearer indication of possible exotic production mechanisms might be available. By using a proton beam, and restricting attention to backward pions, we are clearly probing the ground state properties of the target and not the projectile. We also had in mind covering the transition region from below 1 GeV to the region where the earlier Dubna data[10,11] was taken.

The pion spectra were all found to be exponential in character, with the slope parameter T_0 being weakly dependent on target mass. Figure 28 shows the dependence on energy of the slope parameter T_0 and the ratio $R = \pi^-/\pi^+$ for a Cu target. Both are observed to rise with energy until about 3–4 GeV, after which a leveling off occurs. The dashed curve represents the predictions of an "effective target" model[40] where the incident proton is assumed to interact and excite in a collective fashion the row of nucleons along its path. In de-exciting pions are emitted, much as in thermal models. Although the model agrees nicely with the energy dependence of T_0, it does not reproduce the magnitude of the cross-sections, being low by a factor of 4 at the lower energies. Since the model does not distinguish

between positive and negative pions, it is in disagreement with the π^-/π^+ ratio.

The trends observed in Fig. 28 are common to all targets. Above about 3-4 GeV, a limiting alue is reached. Cross-sections for multi-pion production in N-N collisions are increasing in this region, and could be associated with these limiting features. Detailed calculations, including absorption and charge-exchange effects are needed to ascertain fully the contributions of single-scattering processes in this energy region.

Figure 29 demonstrates the dependence on target mass in this energy region. The cross-sections were parameterized as $\sigma_{inv} \propto A^n$. $K > 1$ corresponds to the cummulative production region.[11] The variations observed in the A-dependence between 0.8 and 4.89 GeV suggest the possibility that different mechanisms are responsible for pion production over this energy region with a smooth evolution from one to the other as the energy is increased.

Finally, our 180° production data provide a definitive test of the hard-scattering model of Schmidt and Blankenbecker.[8] This model, which successfully fit the forward pion production data of Papp et al.,[7] predicts that the 180° negative pion spectrum should be independent of energy, depending only on the scaling parameter x' in the form $(1-x')^N$. Simple counting arguments yield N = 6A-5, so that for a Cu target (A = 63) we expect $\sigma_{inv} \propto (1-x')^{373}$. Figure 30 shows a plot of the invariant cross-section vs. x'. Lack of scaling is evident. However, each spectrum can be represented as $(1-x')^N$, but for values of N much small than predicted (see solid lines through data). Landau and Gyulassy[41] have recently modified this model by assuming that the nucleon interacts with a nucleon cluster, rather

than the entire nucleus. Agreement with the trend of the data is found. The individual clusters are assumed to have internal motion, an exponential distribution providing the best results. They are able to reproduce the data using clusters of one to four nucleons, but with no single choice being preferred.

Recently, Wong and Blankenbecker[42] have generalized the Feynmann scaling variable to massive but weakly bound systems like nuclei, for both proton and pion production. For pion production, they invoke the hard-scattering mechanism schematically shown in Fig. 31. The Dubna[10] and Berkeley[39] results on 180° pion production are compared with this new scaling variable X_H in Fig. 32. The data, spanning the energy range from 0.8-7.51 GeV, do appear to fall on a single curve of the form $(1-X_H)^{88}$; whereas the model predicts $(1-X_H)$.[68] It should also be noted that there is a considerable spread of the data about a single curve. At the present time, the scaling parameter X_H is a somewhat complicated function which does not easily yield to physical interpretation. However, if this new approach holds up, it contains the promise of yielding valuable information on nuclear structure functions.

We have also studied the production of charged pions at 180° with energetic beams of alphas, carbon and argon nuclei. These data are still in a preliminary stage of analysis, but some of the early systematics for the heavier beams are outlined below:

(a) The pion spectra continue to behave approximately in an exponential fashion, with slope parameters 3-5 MeV larger than the case of proton beams.

(b) The ratio, $R = \pi^-/\pi^+$, for the integrated pion yields from a Cu target is ~1 for the carbon beam, and ~1.15 for an argon beam. The increase above R=1 for the argon beam presumably reflects the increased number of neutrons over protons which would favor π^+ production.

(c) The dependence of the integrated pion yields on target (A_t) and projectile (A_p) is found to be, $\sigma \propto (A_p A_t)^{0.8}$.

2) Latest Results from Visual Detectors (Streamer and Bubble Chambers)

In recent years there has been an expanding program to apply visual techniques to the study of nuclear collisions. We next consider some of the recent results coming from these detectors.

A) π-π Correlation Studies

Recently, several groups have applied an intensity interferometric technique to the study of the space and time extent of the source of pion in nucleus-nucleus collisions. This technique was first used in radio-astronomy, and is referred to as the Hanbury-Brown/Twiss effect. The idea of looking for interference effects between pions of identical charge in relativistic nuclear collisions has been pointed out by various authors.[44,45] The observation of such an effect could be an important feature for the study of pion coherence in nuclear matter.

Fung et al.,[43] utilizing the streamer chamber at Berkeley, have studied the correlation between negative pion pairs in both inelastic and central collisions of a 1.8 GeV/nuclear ^{40}Ar beam with various nuclear targets. To look for the correlation, the experimenters have plotted the normalized ratio (R) of the number of negative pion pairs from the same event(s) to the number

of negative pion pairs from different events (D), as suggested by Kopylov.[46] This parameter is shown in Fig. 33, where q represents the relative momentum $(\vec{p}_1-\vec{p}_2)$ between the pion pairs. The rise near q~0 indicates the presence of the interference effect. The solid curve results from fitting the data with a Gaussian space-time distribution for the pion source. The form, suggested by Yano and Koonin,[45] results in the following expression for R:

$$R_D^S(q,E_0) \propto \left(1 + \exp\left[-\left(\frac{\tau E_0}{\sqrt{2}}\right)^2 - \left(\frac{r_0 q}{\sqrt{2}}\right)^2\right]\right) \quad ,$$

where τ and r_0 are the characteristic space-time parameters. The fitted values for τ are found to range from 2-5 x 10^{-24} sec, and $r_0 \sim 4 \pm 1$ fm. Thus, the interference effect is clearly established, and provides a characteristic distance scale which is compatible with the size of the colliding nuclei, and time scale consistent with strong interaction effects. It remains an open question as to whether there is any evidence for coherence which could indicate the presence of exotic pion production mechanisms. Strong final state interactions between the pions and the surrounding matter as they exit the interaction zone will certaintly compound the difficulty in extracting information on the production mechanism. [47]

Bartke[48] has recently reviewed the status of pion production at Dubna using relativistic beams of nuclei up to ^{20}Ne. He reports that in a study of 4.2 GeV/c/nucleon ^{12}C interactions with a Ta plate located inside the 2-meter propane bubble chamber, they find using the like pion interferometric technique, a source size of r = (3.3 ± 0.6)fm, in agreement with the results of Fung et al.[43]

B) Excitation Function for Negative Pion Production

A GSI/LBL/Marburg/ANL collaboration[49] has performed an experiment covering the energy range from 0.4-1.8 GeV/nucleon using the Berkeley streamer chamber. Multi-pion production for the nearly symmetric Ar + KCl system has been studied using both an inelastic (all interactions with ~10 percent bias on events with <5 charged tracks) and central collision trigger. If there are any unusual effects, then a careful study of the energy dependence could reveal their presence. For example, hydrodynamic models predict an increase in the yield of pions at the onset of a phase transition in the dense overlap region of the colliding nuclei.[50] As in a majority of the studies so far, the work discussed here concentrated on the production of negative pions which are very easy to distinguish in the streamer chamber film.

Total charged particle (n_{tot}) and negative pion (n_{π^-}) multiplicity distributions are shown in Fig. 34 for both trigger configurations at 1.8 GeV/nucleon. Notice that for the inelastic trigger (upper points in each graph) $\sigma_{n_{tot}}$ falls off sharply above $n_{tot} \sim 40$. This shoulder at high multiplicities, appears at all bombarding energies, and is not reproduced by either the thermal[22,27] nor cascade models.[51,52] In the thermal model this may be due to the fact that their use of clean-cut geometry neglects dissipation of momentum and energy along the transverse direction, underestimating the number of participants. Correcting for trigger inefficiencies, the total cross section for the inelastic trigger is $\sigma_{inel} = 1.9 \pm 0.1$ b; in agreement with a geometrical reaction cross-section. The total cross-section observed for the central trigger is $\sigma_{central} = 180 \pm$ mb which in a

geometrical model corresponds to impact parameters $b \leq 2.4$ fm. Note that the central collision trigger multiplicity distribution is Gaussian.

Figure 35(a) shows a contour plot of the reaction cross section at 1.8 GeV/nucleon as a function of negative pion and total charged particle multiplicities for the inelastic trigger mode. The reaction products are seen to be confined to a smooth distribution about a narrow ridge. No clear cut evidence for the anomalous production of pions is evident. The dash-dotted curve corresponds to n_{π^-} as a function of n_{tot}, and is seen to be smooth (this was observed at all energies). At high n_{π^-} and n_{tot} the line of complete disintegration is approached. At this point, the colliding nuclei have exploded, with little or no charge bound up in light nuclear fragments. Thus, we see evidence for complete disintegration of these nuclei in central collision events.

A comparison with the number of negative pions and participating protons (Q) can be obtained from the streamer chamber results. Q is defined as follows:

$$Q = n_{tot} - 2n_{\pi^-} - (n^s_{proj} + n^s_{tgt}) ,$$

where n^s refers to the observed spectator fragments from projectile and target. n^s_{proj} was estimated from the number of leading fragments in a 4° cone travelling with beam rapidity, and n^s_{tgt} was estimated from the number of positive tracks with $P_{lab} < 200$ MeV/c. The results are displayed in Fig. 35(b) for the inelastic trigger at 1.8 GeV/nucleon. As indicated by the dots, $\langle n_{\pi^-} \rangle$ increases linearly with Q, as predicted by the

firestreak[27] and cascade[52] models. However, the predicted slopes are larger than those observed. For a given Q, it is found that the square of the dispersion is equal to the mean number of negative pions. This is shown in Fig. 35(c). This result has also been reported by Bartke[48] for ^{12}C central collisions studied at Dubna. These dispersions for the negative pion multiplicities are dominated by fluctuations in pion production and absorption rather than the dispersion associated with elementary N-N pion production processes at these energies.

Figure 36 shows the energy dependence for central collisions of the average negative pion multiplicity in the c.m. frame. A linear dependence of $\langle n_{\pi^-} \rangle$ is observed above 150 MeV/nucleon with a slope of $0.02\pi^-$/(MeV/nucleon). The low energy point falls off this trend, presumably due to effects of Fermi motion which are very important near threshold. Thermal models are not able to reproduce this result, and consistently overestimate pion yields by a factor of 2 or more. A Fermi gas model[53] which assumes thermal but no chemical equilibrium between N's, Δ's, π's, ρ's; is able to reproduce this trend (except near the upper end). To do this, it assumes zero impact parameter and uses the isobar model pion ratios to predict the numbers of negative pions. Absorption effects, including the process, $\Delta + N \rightarrow NN$, are known to reduce the pion yields by as much as 30-50 percent at these energies. Another way of looking at the trend with energy is shown in Fig. 37, where the multiplicity distributions for negative pions for a central trigger are shown for each of the ^{40}Ar energies. Once the bombarding energy is well above the pion threshold, these distributions are approximately Gaussian in shape.

C) Studies With Proton Beams In A Streamer Chamber

In order to gain more insight into hadron-nucleus processes, proton studies using the triggering capability of the streamer chamber have been undertaken. A LeHigh group[54] has studied the interaction of π^+, π^-, and p beams in the 1-3 GeV/c region in the He/Ne gas mixture of the Argonne streamer chamber. Again, because it is much easier to sort out final state π^-'s than π^+'s (which must be clearly separated from the much more prevalent protons), they looked for evidence of isobar formation involving π^-'s. Figure 38 shows the summed monentum distributions π^-'s in the projectile-nucleon c.m. The arrows indicate the momenta associated with the decay of the $\Delta(1232)$ and the N(1470), broad peaks are observed at these values. Further evidence for pions arising from the production and decay of Δ or N* is shown in the π^- angular distribution of Fig. 39, which indicates the presence of J = 3/2 and 5/2 components. Thus, there appears to be reasonably good evidence of pion production via an isobar type mechanism, which is not totally washed out by multiple-scattering and other effects in the case of light targets (He and Ne).

To study in more detail the mechanisms responsible for high energy backward particle production we have supplemented our 180° measurements with a 2.1 GeV proton bombardment of various targets (C, KCl, BaI_2) located in the Berkeley streamer particle.[55,56] The chamber was triggered on any backward particle ($\theta_{LAB} > 90°$), and the resulting film has been scanned and partially measured. Although the analysis is at an earlier stage, there are interesting features that can be reported at this time. First, a large fraction of the events (~50 percent) are found to have an associated negative

track which can be identified as a pion. Typically this pion appears at $\theta_{LAB} < 90^{\circ}$. Thus, backward particle emission (typically the backward track is a proton) at 2.1 GeV is often accompanied by the production of a pion. This suggests that the simple quasi-elastic process, NN→NN, as suggested by Frankel, is not the dominant mechanism at this energy for observed backward protons.

Secondly, there appears to be evidence for the role of pion production followed by absorption in the nuclear environment in the ejection of high energy backward protons.[50] There are two possibilities here:

(a) Production of a pion followed by absorption of the pion on two target nucleons resulting in two back-to-back nucleons, and

(b) Production of the $\Delta^{++}(1232)$ and its subsequent absorption on a target nucleon via, $\Delta+N \rightarrow N+N$, resulting in the emission of two protons which will tend to have a near 180° correlation.

A preliminary study of the correlation of a backward positive track (most likely a proton) and any other positive track shows a correlation function which peaks for 180°. This effect appears not to be explainable by ordinary phase space arguments. Thus, although a pion does not appear in the final state as such, its creation does appear to play a key role as a production mechanism for backward protons. Further studies are continuing with these new data to understand the mechanisms responsible for particle production at backward angles.

SUMMARY OF PRESENT EXPERIMENTS ON PION PRODUCTION

The earlier experiments on inclusive pion spectra have given way to a much larger experimental program measuring pions in the final state. The approach has moved from single-particle inclusive to studies involving correlations (like pion pairs, associated multiplicities, etc). At the same time, model calculations have been developed to explain some of these observations. At present, there is no anomalous signal in these pion measurements which provides irrefutable evidence for any of the phenomena that have been speculated about in A-A collisions, such as: pion condensates, density isomers, large nuclear densities in the overlap region of the colliding systems, etc. However, there is certainly evidence that hot systems are being created in these collisions (with characteristic temperatures of 50-100 MeV). Clearly, geometry and simple N-N collisions are able to explain certain features of the pion results. However, when compared over the complete range of observables (energy, angle, possible correlations, etc.) no single model appears to be favored. Indeed, the thermal models predict an excess of pions in almost all regions of phase space. A confrontation between existing data and models continues to highlight the area of pion production.

FUTURE RESEARCH ON PION PRODUCTION

Now it is time to pull out the crystal ball and attempt to predict future trends in pion production measurements. This can best be accomplished by first considering the near-future, a time zone which will be strongly influenced by existing programs. Then a look into the distant future, with its promise of things yet to come.

Over the period of the next 2-3 years there needs to be a continuing effort on correlation-type measurements. Here such things as the pion interferometry experiments to measure the space-time extent of the source need to be refined. Other examples of correlations include πN effective mass distributions to determine the extent of Δ and N* production as the source of pions in the few GeV/nucleon energy range. Multi-pion production as viewed in the streamer chamber and the GSI/LBL Plastic Ball Project need to be pursued to see how much energy is being deposited in central collision processes in the form of pions. The neutral pion spectrum should be investigated more actively, as it is not subject to the strong Coulomb forces that can plague the charged pions. In all cases, experiments to study pion production in N-N and N-A collisions need to be done, to compare with the A-A results to determine if any exotic phenomena are occurring. The theoretical program needs to address the data in its entirety, and not just certain aspects. For example, a majority of the models are able to reproduce specific trends such as spectral shapes, using widely differing assumptions about the mechanisms involved. But, as we have seen the thermal models are overpredicting the number of pions by a factor of two or so. Is this evidence for an energy crises or the result of transparency?

Finally, we need to keep in mind that by 1982 much heavier beams (up to U) will be available at Berkeley. Clearly the much larger Coulomb fields will play an ever increasing role. Studies of pion production by these massive Coulomb fields will be interesting. Both inclusive and correlation experiments will be required to study the dependence on the Z of the projectile/target. Signals for the exotic states of nuclear matter that

have been speculated about in central collisions have not been readily identified as yet. A signal which is as sharp and clear as the ψ has not turned up. My impression at the moment is that it will be a collection of experimental and theoretical facts, carefully gleaned from the debris of the A-A collisions, that will point the way to these states if they exist.

For the period of >5 years from now, hopefully the new machines[5] which are presently under discussion will be coming on the air. For the higher energy accelerators (>10 GeV/nucleon), pion production can occur not only through Δ,N* mechanisms, but also from the decay of mesonic resonances such as the ω, ρ, f, etc. If one considers the case where colliding beams of nuclei are studied at 20 GeV/nucleon (equivalent to a fixed target energy of ~1 TeV/nucleon) and uses the information on pion multiplicities from the ISR, then in central uranium-uranium collisions we would expect multiplicities of pions approaching 1000. What are the experimental observables we need to exploit? Do we abandon single-particle observables and concentrate on calorimetry (energy flow measurements)? The experimental and theoretical machinery to undertake this will be enormous. But it is at these energies that the quark and gluon degrees of freedom are mainfested. How are they modified or influenced in A-A collisions? These are just the tip of the challenge that will be presented to us at higher energies. A challenge we can not ignore.

ACKNOWLEDGEMENTS

I would like to thank my colleagues at Berkeley who stimulated my thinking on this subject through various discussions; particularly, J. Geaga, J. Harris, S. Chessin, R. Treuhaft, A. Sandoval, S. Nagamiya, M. Gyulassy and J. Rasmussen. Thanks also to L. Madansky for providing me with results on neutral pions before publication. Finally, I would like to thank A. Goldhaber and K. Nakai for inviting me to talk on this subject, and the National Science Foundation for providing travel expenses.

REFERENCES

1. UCRL-20000 NN (August 1970). Compilation of cross-sections for NN and ND interaction above 0.5 GeV/c.
2. D. V. Bugg, A. J. Oxley, J. A. Zoll, J. G. Rushbrooke, V. E. Barnes, J. B. Kinson, W. P. Dodd, G. A. Doran, and L. Riddiford, Phys. Rev. 133, B1017 (1964).
3. G. Alexander, O. Benary, G. Czapek, B. Haber, N. Kidron, B. Reuter, A. Shapira, E. Simopoulon, and G. Yekutieli, Phys. Rev. 154, 1284 (1967).
4. See for example pg. 102 of the April 1978 Particle Data Handbook, published in Phys. Lett. 75B, No. 1 (1978).
5. Several new heavy-ion machines in the GeV/nucleon and above region are under consideration, including: NUKLOTRON in Soviet Union capable of energies up to ~15 GeV/nucleon, NUMATRON in Japan at energies of ~2 GeV/nucleon, SIS 100 at GSI (Darmstadt, West Germany) with energies of ~14 GeV/nucleon, and VENUS at Berkeley with beams up to ~20 GeV/nucleon with both fixed target and colliding beam modes.

6. A. M. Baldin, S. B. Gerasimov, M. Guiordenescu, V. N. Zubarev, L. K. Ivanova, A. D. Kirillov, V. A. Kuznetsov, N. S. Moroz, V. B. Radomanov, V. N. Ramzhin, V. S. Stavinskii, and M. Yatsuta, Yad. Fiz. 18, 79 (1973); (Sov. J. Nucl. Phys. 18, 41 (1974).

7. J. Papp, J. Jaros, L. Schroeder, J. Staples, H. Steiner, A. Wagner, and J. Wiss, Phys. Rev. Letters 34, 601 (1975).

8. I. A. Schmidt and R. Blankenbecler, Phys. Rev. D15, 3321 (1977).

9. W. Schimmerling, K. G. Vosburgh, K. Koepke, and W. Wales, Phys. Rev. Letters 33, 1170 (1974).

10. A. M. Baldin, N. Giordenescu, V. N. Zubarev, L. K. Ivamova, and V. S. Stavinskii, Yad. Fiz. 20, 1201 (1975) [Sov. J. Nucl. Phys. 20, 629 (1976)].

11. A. M. Baldin in Proceedings of the 19th International Conference on High Energy Physics, Tokyo, Japan, 1978, edited by G. Takeda, S. Homma, M. Kawaguchi, and H. Miyazawa (Physical Society of Japan, Tokyo, 1979), pg. 455.

12. V. V. Burov, V. K. Lukyanov, and A. I. Titov, Phys. Lett. 67B, 46 (1977).

13. M. I. Gorenstein and G. M. Zinovjev, Phys. Lett. 67B, 100 (1977).

14. M. B. Mathis and Meng Ta-chung, Phys. Rev. C18, 952 (1978).

15. L. L. Frankfurt and M. I. Strikman, Phys. Lett. 83B, 407 (1979).

16. T. Mayashiro, O. Kusumoto, G. Fujioka, M. Fukushima, and T. Hara, Lett. Nuovo Cimento 16, 71 (1976).

17. J. Cronin, et al., Phys. Rev. D11, 3105 (1975).

18. L. S. Schroeder, Nucl. Instr. and Meth. 162, 395 (1979).

19. S. Y. Fung, W. Gorn, G. P. Kiernan, F. F. Liu, J. J. Lu, Y. T. Oh, J. Ozawa, R. T. Poe, L. Schroeder, and H. Steiner, Phys. Rev. Lett. 40, 292 (1978).

20. J. P. Vary, Phys. Rev. Lett. 40, 295 (1978).

21. M. Gyulassy and S. K. Kauffmann, Phys. Rev. Lett. 40, 298 (1978).

22. G. D. Westfall et al., Phys. Rev. Lett. 37, 1202 (1976); J. Gosset et al., Phys. Rev. C16, 629 (1977).

23. Y. Afek, G. Berlad, A. Dar, and G. Eilam, Phys. Rev. Lett. 41, 849 (1978).

24. Y. Afek et al., in Multiparticle Production on Nuclei at Very High Energies, edited by G. Bellini, L. Bertocchi, and P. G. Rancoita (International Centre for Theoretical Physics, Trieste, 1977, p. 591 and references therein).

25. A. M. Baldin, in Proceedings of the Seventh International Conference on High-Energy Physics and Nuclear Structure, Zurich, Switzerland, 1977, edited by M. P. Locher (Birkhauser-Verlag, Basil and Stuttgart, 1977).

26. I. Tanihata, S. Nagamiya, O. Chamberlain, M.-C. LeMaire, S. Schnetzer, G. Shapiro, and H. Steiner, Phys. Lett. 87B, 349 (1979). See also S. Nagamiya, p. 71 of the 4th High Energy Heavy Ion Summer Study, July 24-28, 1978 (LBL) - LBL-7766 (CONF-780766).

27. J. Gosset, J. I. Kapusta and G. D. Westfall, Phys. Rev. C18, 844 (1978).

28. R. L. Hatch and S. E. Koonin, Phys. Lett. 81B, 1 (1979).

29. S. Frankel, Phys. Rev. Lett. 38, 1338 (1977).

30. P. Siemens and J. O. Rasmussen, Phys. Rev. Lett. 41, 880 (1979).

31. J. Chiba, K. Nakai, I. Tanihata, S. Nagamiya, H. Bowman, J. Ingersoll, and J. O. Rasmussen, Phys. Rev. C20, 1332 (1979); and K. Nakai, J. Chiba, I. Tanihata, H. Sasao, H. Bowman, S. Nagamiya, and J. O. Rasmussen, Phys. Rev. C20, 2210 (1979).

32. K. L. Wolf, H. H. Gutbrod, W. G. Meyer, A. M. Poskanzer, A. Sandoval, R. Stock, J. Gosset, C. H. King, G. King, Nguyen Van Sen, and G. D. Westfall, Phys. Rev. Lett. 42, 1448 (1979).

33. K. G. Libbrecht and S. E. Koonin, Phys. Rev. Lett. 43, 1581 (1979).

34. H. Bowman and J. O. Rasmussen, private communication.

35. W. Benenson, G. Bertsch, G. M. Crawley, E. Kashy, J. A. Nolen, Jr., H. Bowman, J. G. Ingersoll, J. O. Rasmussen, J. Sullivan, M. Koike, J. Peter, and T. E. Ward, Phys. Rev. Lett. 43, 683 (1979).

36. G. Bertsch, Phys. Rev. C15, 713 (1977).

37. W. DeJarnette, T. Hallman, E. McIntyre, J. C. Walker, L. Madansky, J. Carroll, A. Sagle, and R. J. Semper, Johns Hopkins preprint (1980).

38. E. Aslanides, P. Fassnacht, F. Hibou, E. Chiavassa, G. Dellacasa, M. Gallio, A. Musso, T. Bressani, and G. Puddu, Phys. Rev. Lett. 43, 1466 (1979).

39. L. S. Schroeder, S. A. Chessin, J. V. Geaga, J. Y. Grossiord, J. W. Harris, D. L. Hendrie, R. Treuhaft, and K. Van Bibber, Phys. Rev. Lett. 43, 1787 (1979).

40. H. B. Mathis and Meng Ta-chung, Phys. Rev. C18, 952 (1978).

41. R. H. Landau and M. Gyulassy, Phys. Rev. C19, 149 (1979).

42. C. Y. Wong and R. Blankenbecker, ORNL preprint, "Scaling Phenomena in Relativistic Nucleus-Nucleus Collisions," April 1980, and C. Y. Wong, private communication.

43. S. Y. Fung, W. Gorn, G. P. Kiernan, J. J. Lu, Y. T. Oh, and R. T. Poe, Phys. Rev. Lett. 41, 1592 (1978).

44. M. Gyulassy, S. K. Kauffmann, and Lance Wilson, Phys. Rev. C20, 2267 (1979).

45. F. B. Yano and S. E. Koonin, Phys. Lett. 78B, 556 (1978).

46 G. I. Kopylov, Phys. Lett. 50B, 472 (1974).

47. M. Gyulassy, private communication.

48. J. Bartke, in Proceedings of the 8th International Conference on High Energy Physics and Nuclear Structure, Vancouver, August (1979), D. F. Measday and A. W. Thomas (eds.), North Holland; and published in Nucl. Phys. A335, 481 (1980).

49. A. Sandoval, R. Stock, H. E. Stelzer, R. E. Renfordt, J. W. Harris, J. P. Brannigan, J. V. Geaga, L. J. Rosenberg, L. S. Schroeder, and K. L. Wolf, LBL-10830, submitted to Phys. Rev. Lett. (May, 1980).

50. H. Stocker, J. Maruhn and W. Greiner, Z. Physik A286, 121 (1978) and Phys. Lett. 81B, 303 (1979).

51. Y. Yariv and Z. Frankel, Phys. Rev. C20, 2227 (1979).

52. J. Cugon, T. Mizutani, and J. Vandermeulen, Cal. Tech. Report MAP-10 (1980).

53. I. Montvay and J. Zimanyi, Nucl. Phys. A316, 490 (1979).

54. R. Allen, A. Kanofsky, M. Abul Hasan, LeHigh, University Report, "A Study of Inelastic Particle-Nuclei Reactions in a Large Streamer Chamber," 1979 (LEH-HEP. 79-4-1), unpublished.

55. LBL/GSI Steamer Chamber Collaboration: J. W. Harris, J. Brannigan, J. V. Geaga, L. S. Schroeder, R. N. Treuhaft, A. Sandoval, H. E. Stelzer, and R. Stock (Experiment 400H at the Bevalac).

56. J. W. Harris, to be published in the proceedings of the "Winter Workshop on Nuclear Dynamics," held at Granlibakken, California, March 17–21, 1980.

FIGURE CAPTIONS

Fig. 1. p-p cross-sections, (a) σ_T and σ_{el} vs. beam momentum (GeV/c), (b) σ_T and σ_{el} momentum interval, $0.5 < p_{lab} < 5.5$ GeV/c, with arrows indicating position of various thresholds. Figures taken from UCRL-2000(NN) August 1970.

Fig. 2. Measured cross sections for (a) $pp \to pn\pi^+$ and $pp\pi^\circ$, (b) $pp \to pp\pi^+\pi^-$, as function of beam momentum. Figures taken from UCLRL-2000 (NN) August 1970.

Fig. 3. (a) Q-value distribution for π^+p pairs from $pp \to pn\pi^+$ at 970 MeV (Ref. 2); where solid curve is the prediction of phase space and dashed curve the isobar model prediction, normalized to the total number of events, and

(b) Invariant mass distribution of $p\pi^+$ in the reaction $pp \to pn\pi^+$ at 4.64 GeV (Ref. 3).

Fig. 4. Representation of $\sigma_T(\pi^\pm p)$ as a function of pion beam momentum.

Fig. 5. Invariant cross section for negative pion production at 2.5°(Lab) (a) incident proton (1.05-4.2 GeV), (b) incident deuterons and alphas (1.05 and 2.1 GeV/nucleon). Data from Ref. 7.

Fig. 6. (a) The X_F spectrum compared to the carbon data (Ref. 7) illustrating scaling, and

(b) Deuteron beam data to $(1-X_F)^N$, with N=9 (the value favored for vector-meson exchange with monopole form factors). These counting rules are the same as quark counting (Ref. 8).

Fig. 7. Invariant cross section for negative pion production at 2.5°(Lab) for 1.05 and 2.1 GeV/nucleon (a) deuteron and (b) alpha beams. The solid line represents the prediction of model discribed in text (also see Ref. 7).

Fig. 8. A-Dependence of cross section assuming $\sigma \propto A^n$, where A = target mass.

Fig. 9. (a) Invariant cross section/nucleon versus T_π (Ref. 11) for pA → $\pi^-(180°)$ + X, and
(b) A-dependence for 180° $\pi^\pm$ yields assuming $\sigma \propto A^n$.

Fig. 10. Central collision of a 1.8 GeV/nucleon ^{40}Ar projectile with a Pb_3O_4 target located inside the LBL streamer chamber.

Fig. 11. Negative-pion multiplicity for (a) 1.8 GeV/nucleon ^{40}Ar and (b) 2.1 GeV/nucleon ^{12}C beams incident on LiH and Pb_3O_4.

Fig. 12 (a) π^- multiplicity distribution for Ar + Pb_3O_4 at 1.8 GeV/nucleon: closed circles, data from Ref. 19; triangles, Ref. 20, and solid curves predictions of thermal model of Ref. 21. (b) π^- multiplicity distribution as a function of impact parameter b for Ar + Pb at 1.8 GeV/nucleon, taken from Ref. 21.

Fig. 13. Comparison between experimental results[19] and the CTM predictions (Ref. 23) for multiplicity distributions of π^- produced in various nucleus-nucleus collisions. Shaded areas reflect uncertainly in the input experimental data on $\langle n_-(Q)\rangle$ in pp collisions.

Fig. 14. Comparison between experimental results[25] (closed circles) and the CTM predictions (Ref. 23) in α-nucleus collisions at 17.8 GeV/c. The open circles are the result of normalizing the experimental results to the CTM prediction for $P(n_- = 0)$.

Fig. 15. Plot of $\langle n_{\pi^-}\rangle \sigma_{N_{\pi^-}}/\sigma_{inel}$ vs $N_{\pi^-}/\langle n_{\pi^-}\rangle$ for data of Ref. 19 on multiplicity distribution of π^-'s in A-A collisions.

Fig. 16. Contour plots of invariant cross-sections in the nucleon-nucleon c.m. frame for the data of Ref. 26. The top graph corresponds to Ar + KCl → π^- + X and the bottom to Ar + Pb → π^- + X, both at 800 MeV/nucleon.

Fig. 17. Energy distributions for the data of Ref. 26 for π^-'s produced at 90°* in the N-N c.m. frame. E_0 values obtained from fit of data to $e^{-E_k^*/E_0}$. The predictions of the firestreak (Ref. 27) and hard-scattering models (Ref. 28) are compared with the Ne + NaF → π^- + X data.

Fig. 18. Energy dependence of the slope parameter E_0 for negative pions and protons for data of Ref. 27. Model calculations are compared with the data.

Fig. 19. Energy dependence of the integrated cross section $d\sigma/d\Omega$ for negative pions and protons from data of Ref. 27. Thermal (solid line) and hard-scattering (CKO - dashed line) model calculations are indicated.

Fig. 20. Pion momentum distributions at $\theta_\pi^{c.m.} = 90°$ and 150°. Solid points are data from Ref. 27, open points are data from Ref. 31.

Fig. 21 Contour plots of the invariant cross sections (a) for ^{20}Ne + NaF $\rightarrow \pi^{\pm}$ + X at 800 MeV/nucleon, and (b) for p + p $\rightarrow \pi^{+}$ + X at 730 MeV. Numbers next to solid lines are value of cross section in mb/sr GeV/c. Dots are the measured points. Contour lines should be symmetric about $\theta_{\pi}^{c.m.} = 90°$

Fig. 22. Contours of constant invariant cross section in $p_{\perp}/m_{\pi}c$ and rapidity (y) plane for (a) ^{40}Ar + $^{40}Ca \rightarrow \pi^{+}$ + X at 1.05 GeV/nucleon and (b) p + p $\rightarrow \pi^{+}$ + X at 730 MeV. The ^{40}Ar data points have been reflected about the mid-rapidity axis.

Fig. 23 Experimental data for ^{40}Ar + $^{40}Ca \rightarrow \pi^{+}$ + X at 1.05 GeV/nucleon (upper left-hand corner) and results of model calculation of Ref. 33 to study effects of the coulomb field on the pion spectra.

Fig. 24. Ratio (R) of the π^{-} to π^{+} cross section in Ne + NeF $\rightarrow$ $\pi^{\pm}(0°)$ + X as a function of the pion kinetic energy in projectile rest frame (Ref. 35). Solid curve shows the Coulomb ratios calculated in projectile frame.

Fig. 25. Pion production cross section (Ne + NaF $\rightarrow \pi(0°)$ + X) versus pion rapidity for data of Ref. 35. Solid curve are thermal model predictions, and the dashed lines predictions of a first-chance collision model (Ref. 36).

Fig. 26. Various cross sections versus beam energy for ^{12}C + Pb collisions from Ref. 37. The different symbols correspond to various multiplicity cuts made on the data.

Fig. 27. Inclusive π^{-} spectrum (^{3}He + $^{6}Li \rightarrow \pi^{-}$ + X at 910 MeV). Inset shows more detail of the p_{π} region from 680-750 MeV/c.

Fig. 28. Energy dependence of (a) T_0 parameter for pions, and (b) the π^-/π^+ ratio at 180° obtained by integrating each spectra up to 100 MeV for p-Cu collisions from 0.8-4.89 GeV (Ref. 39). The dashed curve in both cases refers to the predictions of the "effective-target" model (Ref. 40).

Fig. 29. A-dependence for charge-pion production. The data (Ref. 39) were fitted by the form A^n; the exponent n is plotted vs the ratio K for (a) 0.8 and 1.05 GeV, (b) 2.1 GeV, and (c) 4.89 GeV protons.

Fig. 30. Lorentz-invariant cross section vs X' for π^- production at 180° by 0.8, 1.05, 2.1, and 4.89 GeV protons and π^+ production at 180° by 3.5 GeV protons on a Cu target (Ref. 39).

Fig. 31. Hard-scattering process giving rise to pion production at 180°.

Fig. 32. Experimental invariant corss section for p + Cu → $\pi^{\pm}$(180°) + X plotted as a function of the scaling variable X_H.

Fig. 33. Kopylov ratio versus relation pion momentum q.

Fig. 34. Multiplicity distributions for total charged particles (n_{tot}) and negative pions ($n_{\pi}-$) in 1.8 GeV/nucleon Ar + KCl collisions. Upper points correspond to the inelastic trigger and lower to the central collision trigger. Solid curves are a guide-to-the-eye only.

Fig. 35. Topology of reaction products for Ar + KCl in the inelastic trigger mode at 1.8 GeV/nucleon, drawn as contours of constant cross-section (mb) in the $n_{\pi}-$, n_{tot} plane. (b) Contour plot of the same reaction in the $n_{\pi}-$ vs Q(number participant protons) plane. (c) Plot of the square of the dispersion ($D_{\pi}-^2$) vs $\langle n_{\pi}- \rangle$, where $D_{\pi}- = \sqrt{\langle n^2_{\pi-} \rangle - \langle n_{\pi-} \rangle^2}$.

Fig. 36. Energy dependence of $\langle n_{\pi^-} \rangle$ for central collisions. The incident energy is plotted in the c.m. frame.

Fig. 37. Multiplicity distributions for π^-'s produced in ^{40}Ar + KCl central collisions as function of energy.

Fig. 38. Momentum distributions (summed over all beams) for final state π^-'s in the beam particle-nucleon c.m. frame. Results are for interaction in the He and Ne of the steamer chamber.

Fig. 39. Angular distribution of π^-'s in beams particle-nucleon c.m. frame.

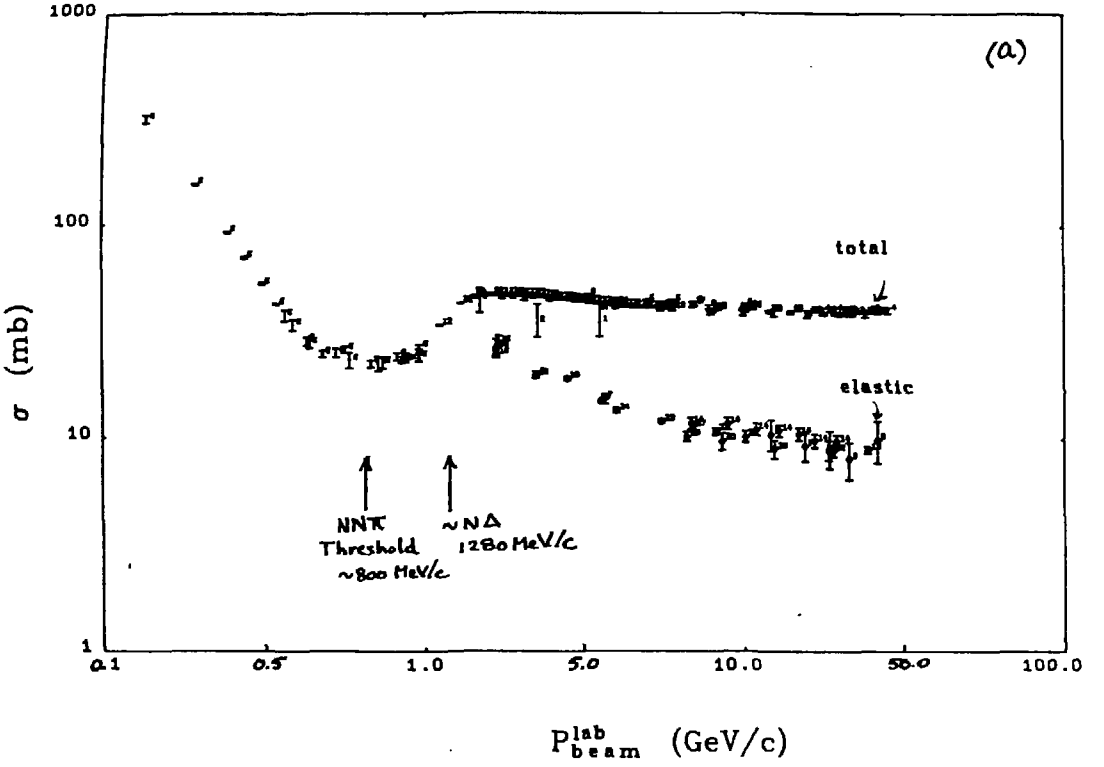
(a)
σ (mb)
1000
100
10
1
total
elastic
NNπ
Threshold
~800 MeV/c
~NΔ
1280 MeV/c
0.1
0.5
1.0
5.0
10.0
50.0
100.0
P lab beam (GeV/c)

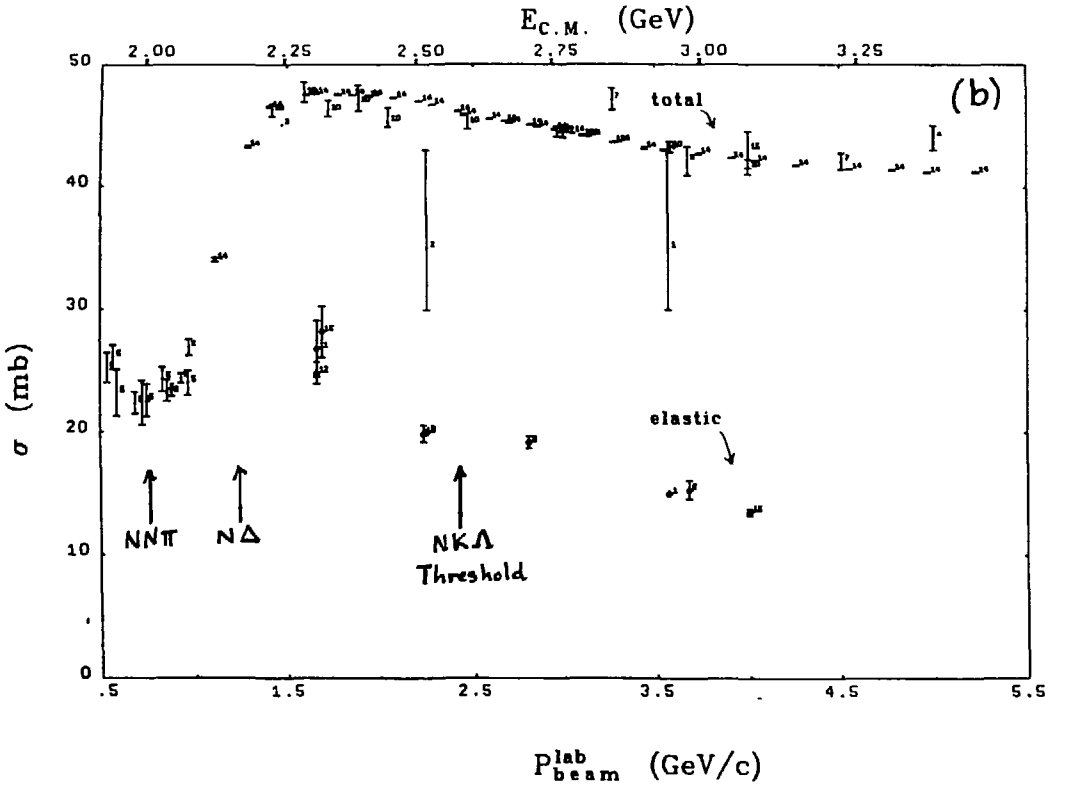
E C.M. (GeV)
2.00
2.25
2.50
2.75
3.00
3.25
(b)
σ (mb)
50
40
30
20
10
0
total
elastic
NNπ
NΔ
NKΛ
Threshold
.5
1.5
2.5
3.5
4.5
5.5
P lab beam (GeV/c)

Fig. 1

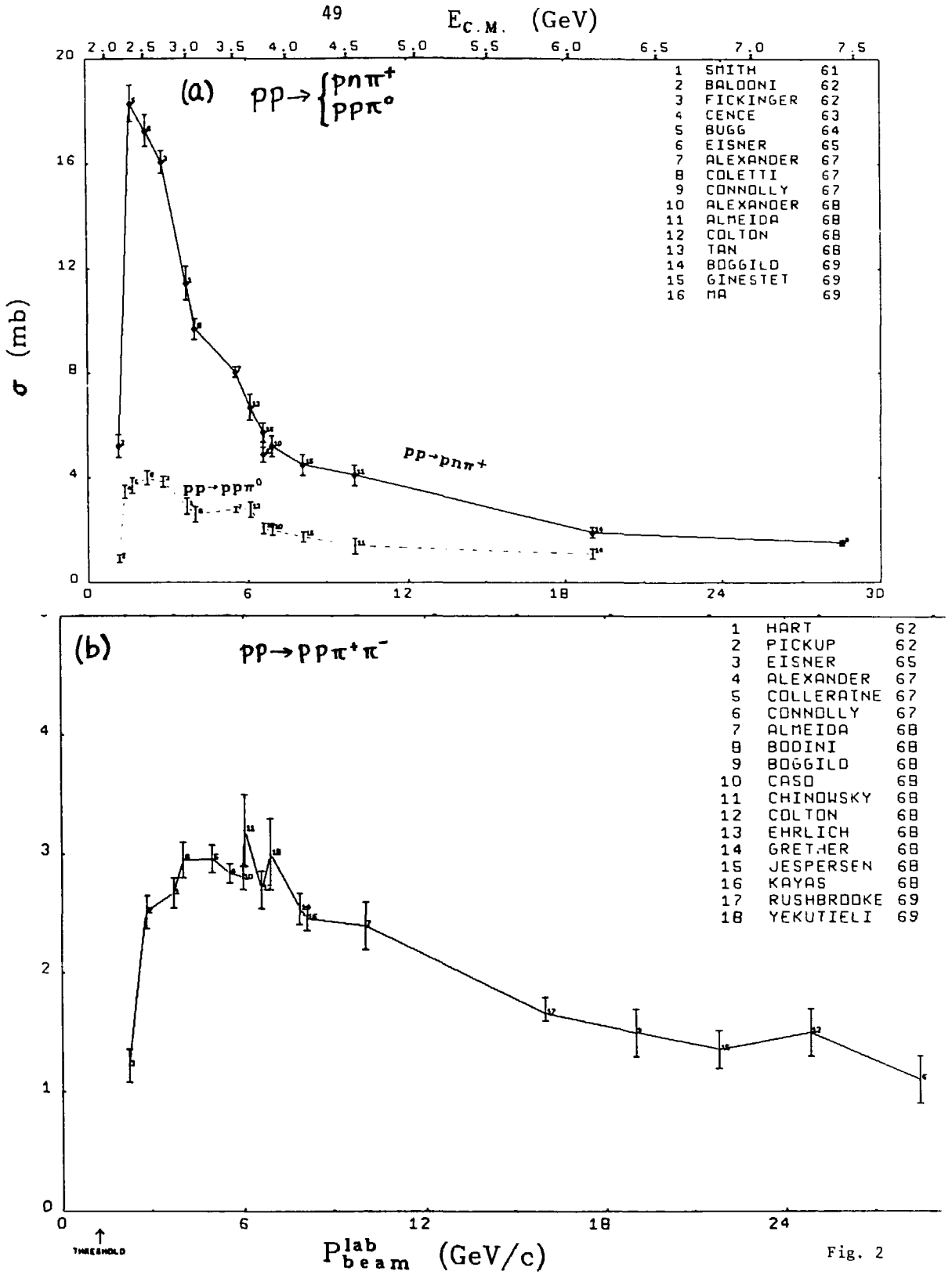
$E_{C.M.}$ (GeV)
(a)
$pp \rightarrow \begin{cases} pn\pi^+ \\ pp\pi^0 \end{cases}$
1 SMITH 61
2 BALDONI 62
3 FICKINGER 62
4 CENCE 63
5 BUGG 64
6 EISNER 65
7 ALEXANDER 67
8 COLETTI 67
9 CONNOLLY 67
10 ALEXANDER 68
11 ALMEIDA 68
12 COLTON 68
13 TAN 68
14 BOGGILD 69
15 GINESTET 69
16 MA 69
$pp \rightarrow pn\pi^+$
$pp \rightarrow pp\pi^0$
σ (mb)
(b)
$pp \rightarrow pp\pi^+\pi^-$
1 HART 62
2 PICKUP 62
3 EISNER 65
4 ALEXANDER 67
5 COLLERAINE 67
6 CONNOLLY 67
7 ALMEIDA 68
8 BODINI 68
9 BOGGILD 68
10 CASO 68
11 CHINOWSKY 68
12 COLTON 68
13 EHRLICH 68
14 GRETHER 68
15 JESPERSEN 68
16 KAYAS 68
17 RUSHBROOKE 69
18 YEKUTIELI 69
σ (mb)
THRESHOLD
P^{lab}_{beam} (GeV/c)

Fig. 2

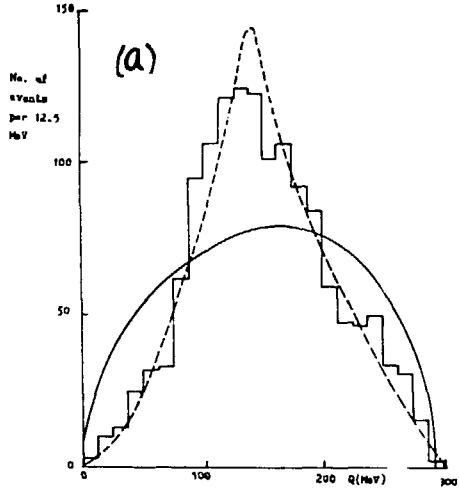
(a)
No. of events per 12.5 MeV
150
100
50
0
0
100
200
Q(MeV)
300
$Q = M(\pi N) - (M_\pi + M_N)$

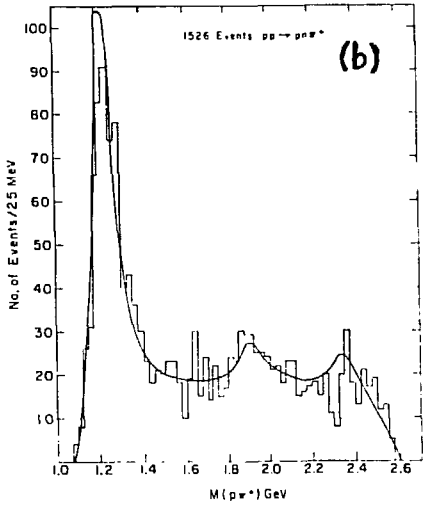
1526 Events
(b)
No. of Events/25 MeV
100
90
80
70
60
50
40
30
20
10
1.0
1.2
1.4
1.6
1.8
2.0
2.2
2.4
2.6
M(pω*) GeV

Fig. 3

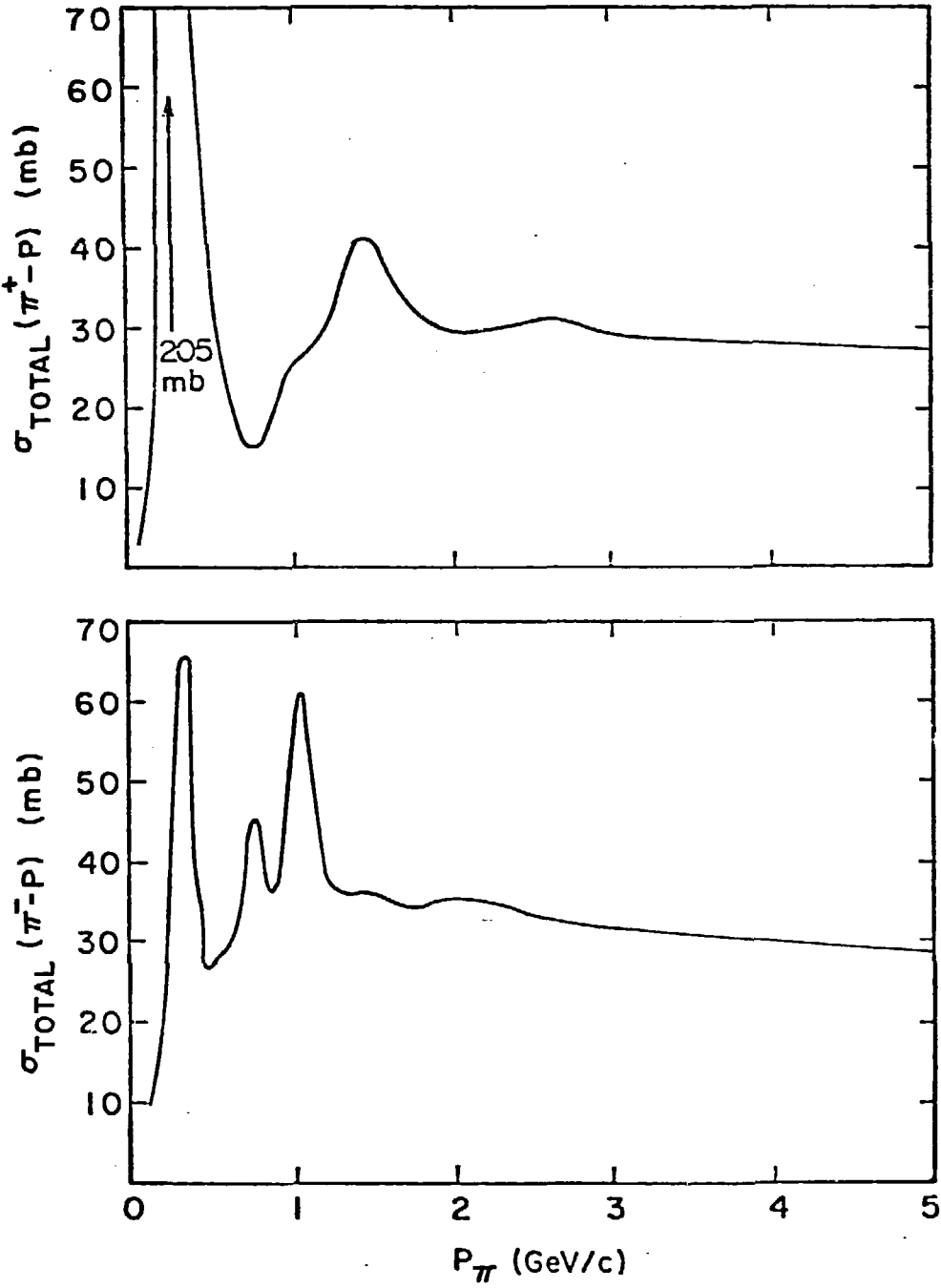
70
60
50
40
30
20
10
$\sigma_{TOTAL}(\pi^+-P)$ (mb)
205
mb
70
60
50
40
30
20
10
$\sigma_{TOTAL}(\pi^--P)$ (mb)
0
1
2
3
4
5
P_π (GeV/c)

Fig. 4

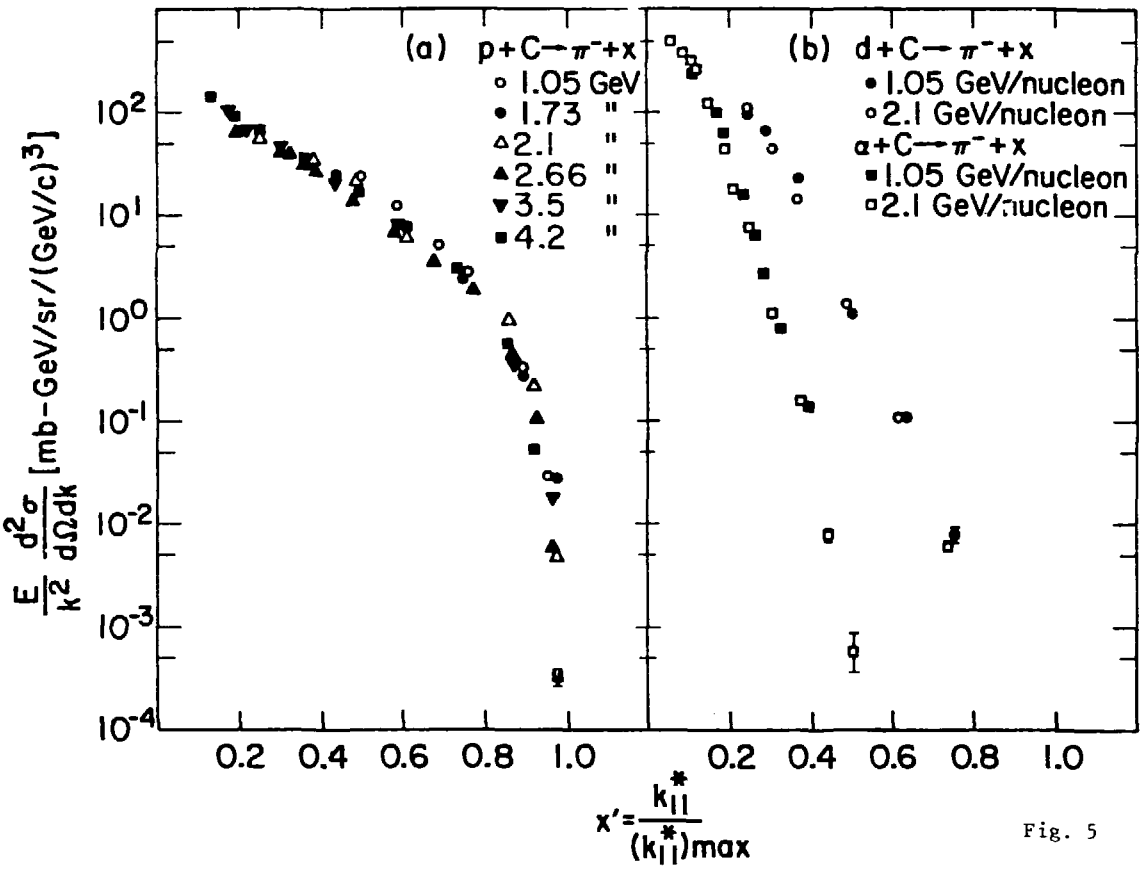
(a) p+C→π⁻+x
1.05 GeV
1.73 "
2.1 "
2.66 "
3.5 "
4.2 "
(b) d+C→π⁻+x
1.05 GeV/nucleon
2.1 GeV/nucleon
α+C→π⁻+x
1.05 GeV/nucleon
2.1 GeV/nucleon
E/k² d²σ/dΩdk [mb-GeV/sr/(GeV/c)³]
x'=k*₁₁/(k*₁₁)max

Fig. 5

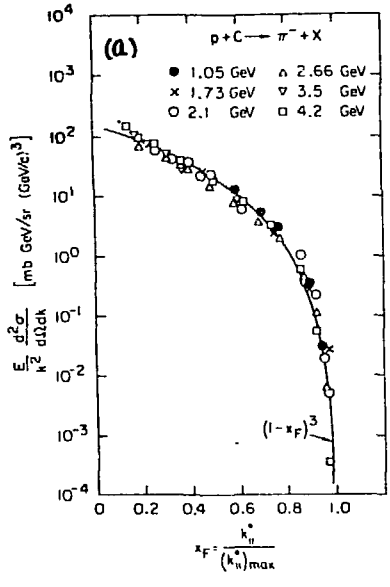
(a)
p+C→π⁻+X
1.05 GeV
1.73 GeV
2.1 GeV
2.66 GeV
3.5 GeV
4.2 GeV
(1-x_F)³
x_F = k*₁₁/(k*₁₁)max

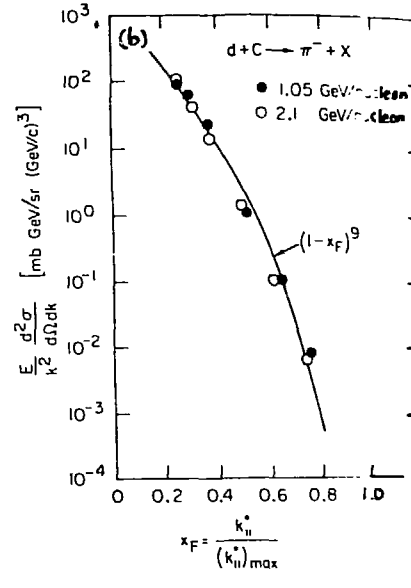
(b)
d+C→π⁻+X
1.05 GeV/nucleon
2.1 GeV/nucleon
(1-x_F)⁹
x_F = k*₁₁/(k*₁₁)max

Fig. 6

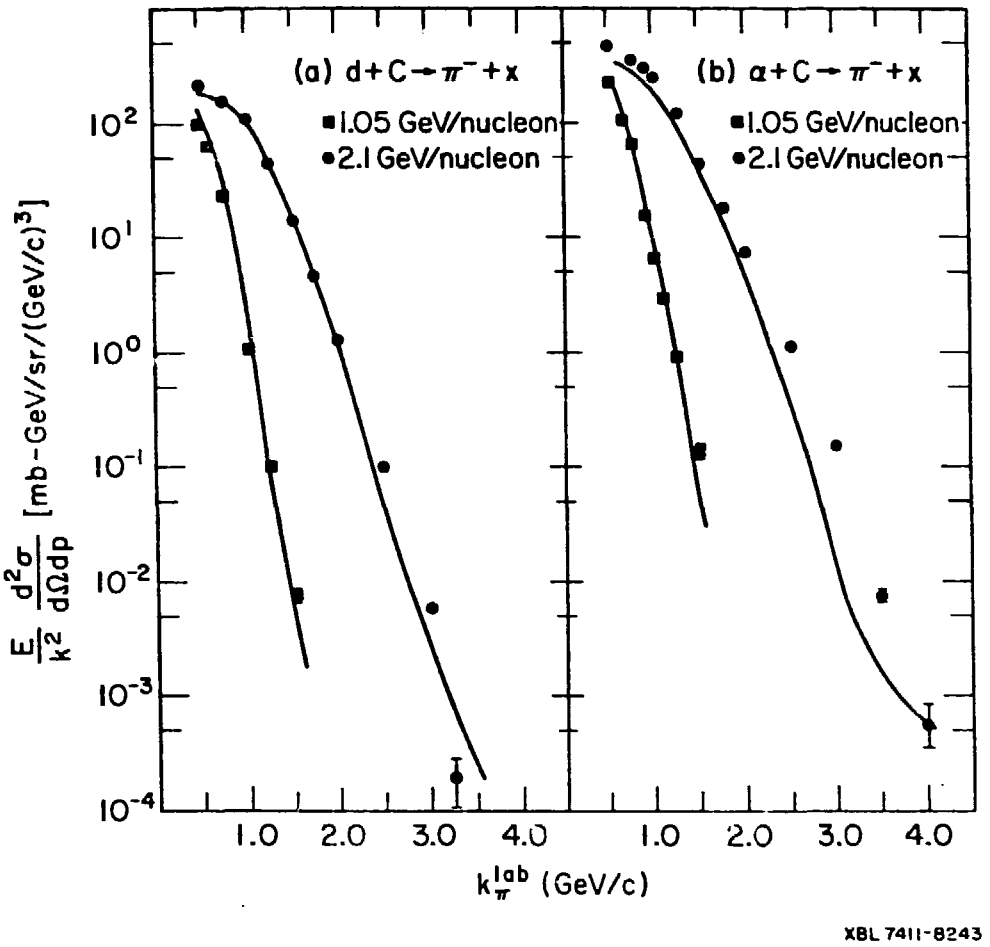
(a) d+C→π⁻+x
■1.05 GeV/nucleon
●2.1 GeV/nucleon
(b) α+C→π⁻+x
■1.05 GeV/nucleon
●2.1 GeV/nucleon
$\frac{E}{k^2}\frac{d^2\sigma}{d\Omega dp}$ [mb-GeV/sr/(GeV/c)³]
10^2
10^1
10^0
10^{-1}
10^{-2}
10^{-3}
10^{-4}
1.0
2.0
3.0
4.0
k_π^{lab} (GeV/c)
XBL 7411-8243

Fig. 7

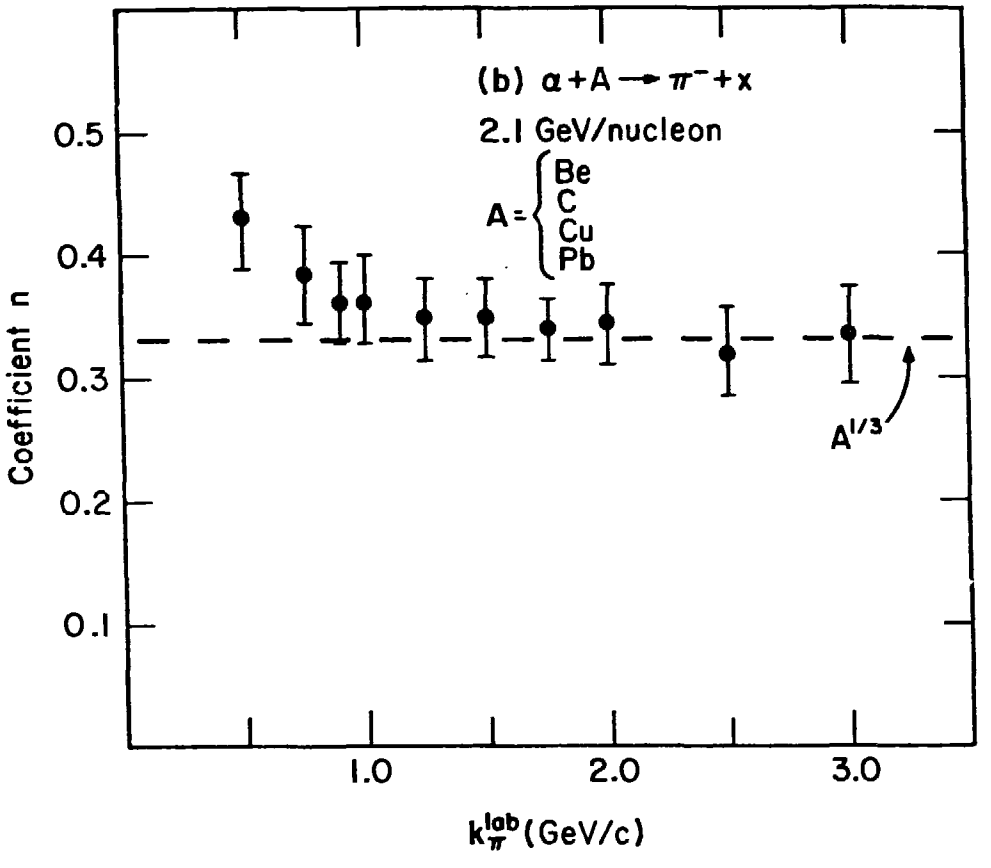
(b) α+A → π⁻+x
2.1 GeV/nucleon
A = Be
C
Cu
Pb
A^1/3
Coefficient n
0.5
0.4
0.3
0.2
0.1
1.0
2.0
3.0
k_π^lab (GeV/c)
XBL748-3900

Fig. 8

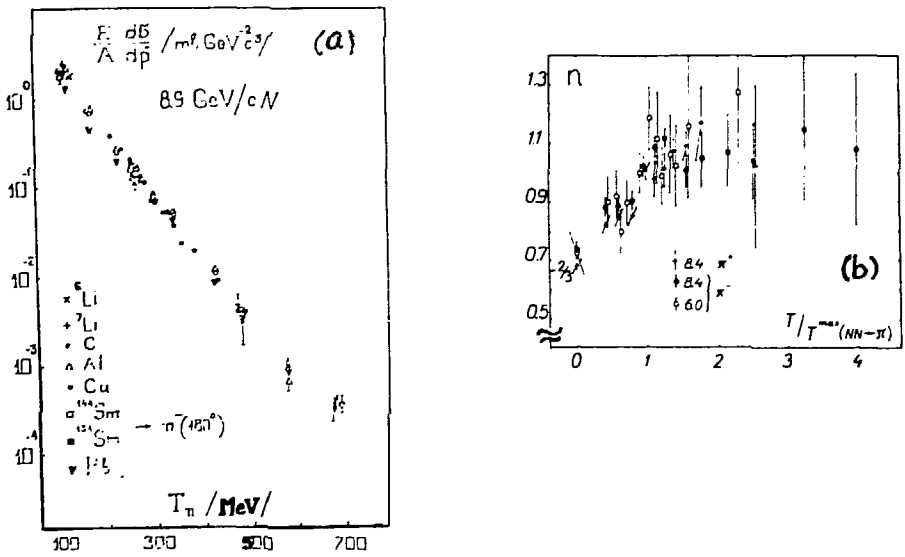

Fig. 9

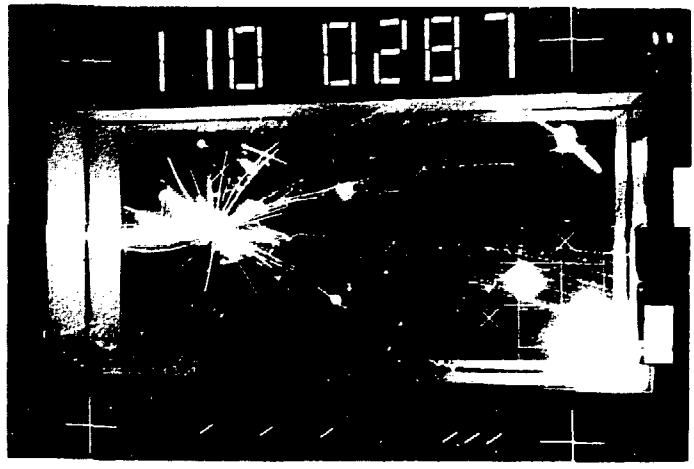

XBB 750-8445

Fig. 10

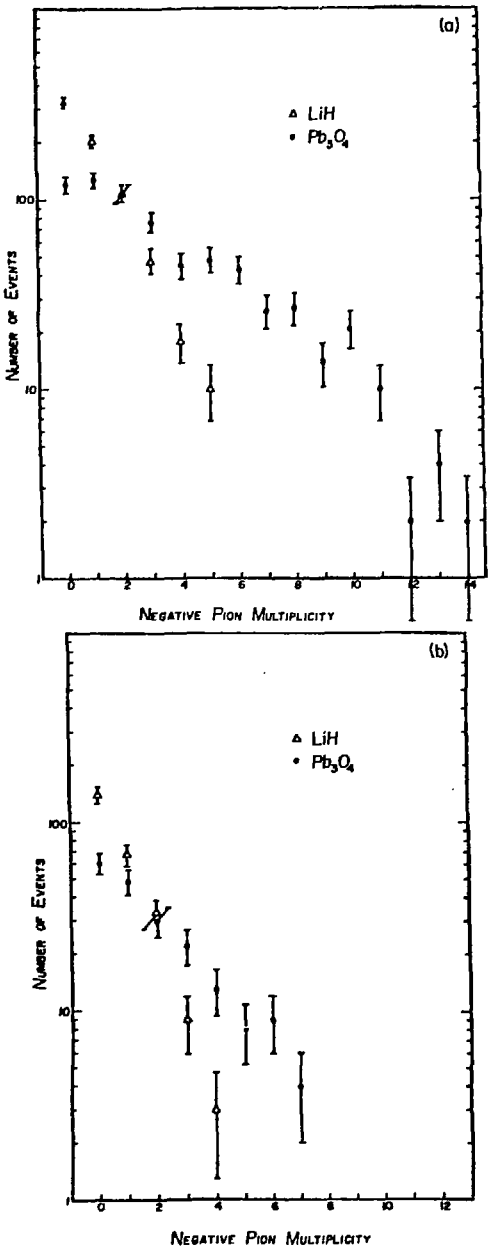
(a)
Δ LiH
• Pb_3O_4
Number of Events
Negative Pion Multiplicity
(b)
Δ LiH
• Pb_3O_4
Number of Events
Negative Pion Multiplicity

Fig. 11

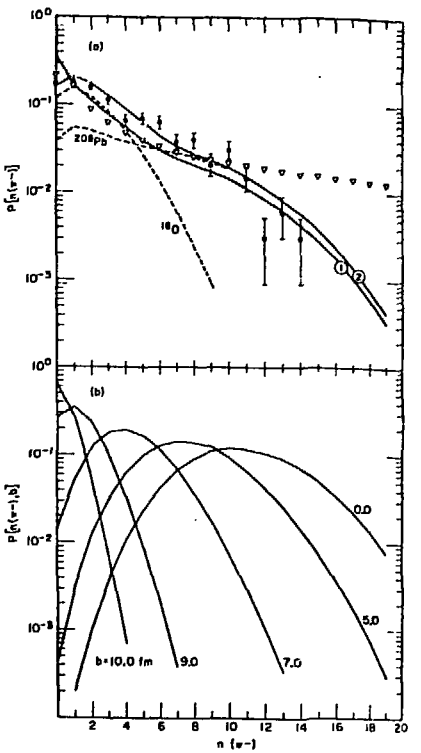
(a)
^{208}Pb
^{16}O
(b)
b=10.0 fm
9.0
7.0
5.0
0.0
n (π⁻)

Fig. 12

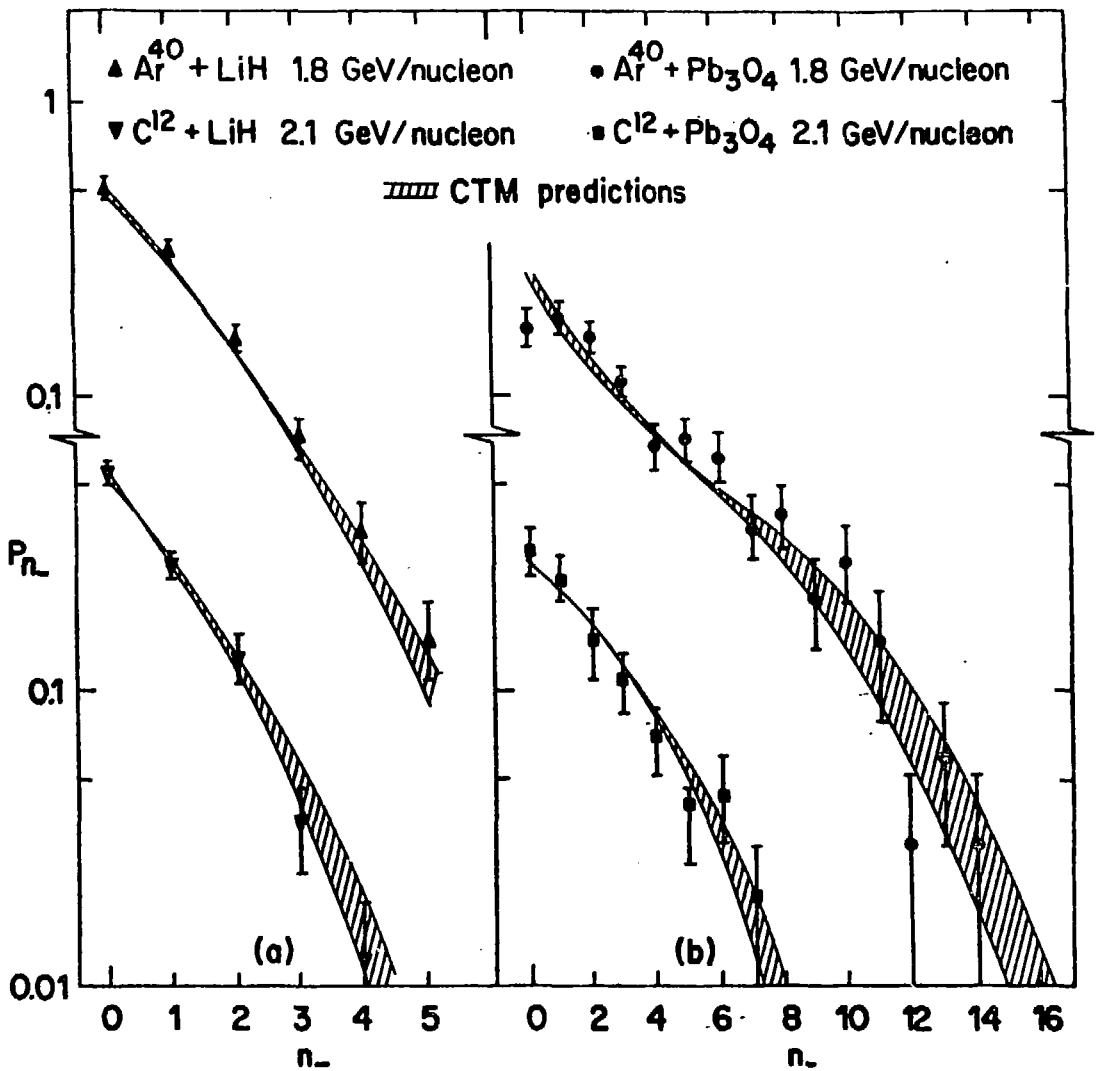
▲ Ar^{40} + LiH 1.8 GeV/nucleon
● Ar^{40} + Pb_3O_4 1.8 GeV/nucleon
▼ C^{12} + LiH 2.1 GeV/nucleon
■ C^{12} + Pb_3O_4 2.1 GeV/nucleon
CTM predictions
P_{n_-}
1
0.1
0.01
(a)
(b)
0 1 2 3 4 5
0 2 4 6 8 10 12 14 16
n_-
n_-

Fig. 13

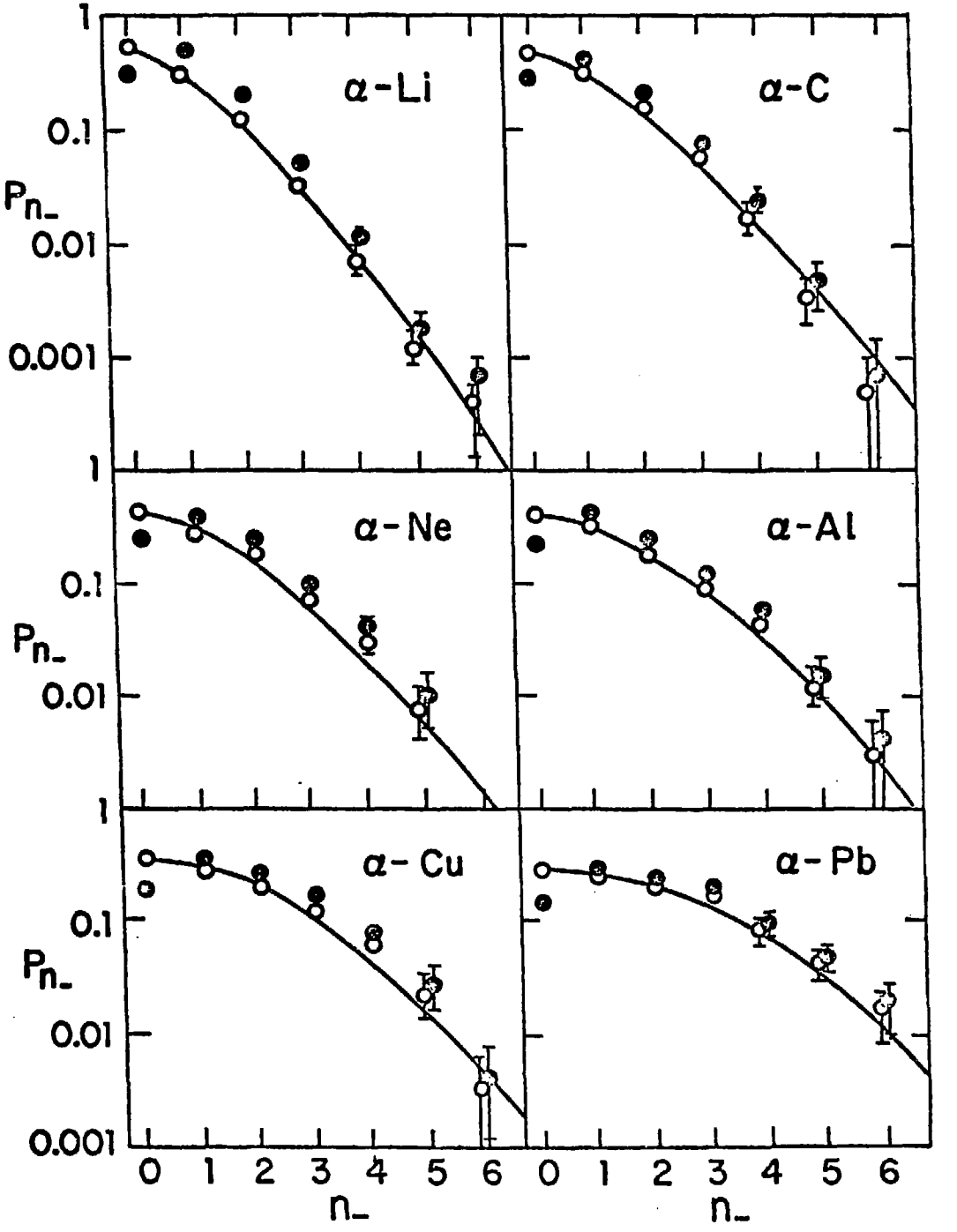

Fig. 14

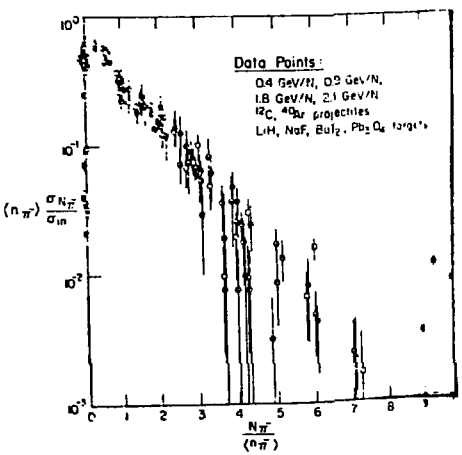

Fig. 15

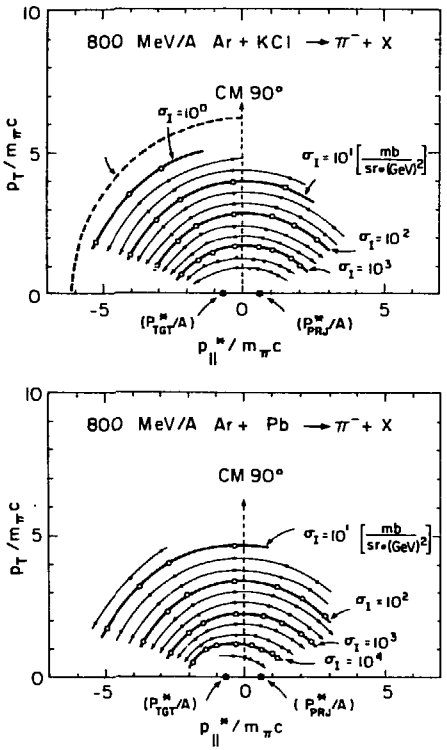

Fig. 16

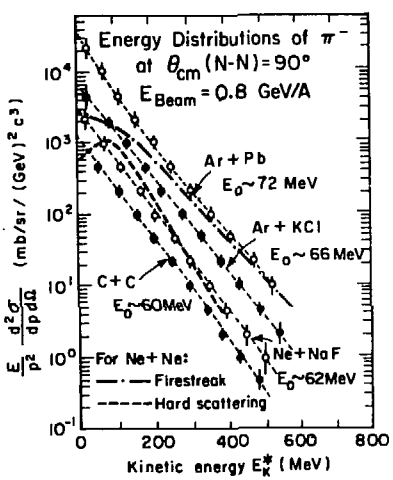

Fig. 17

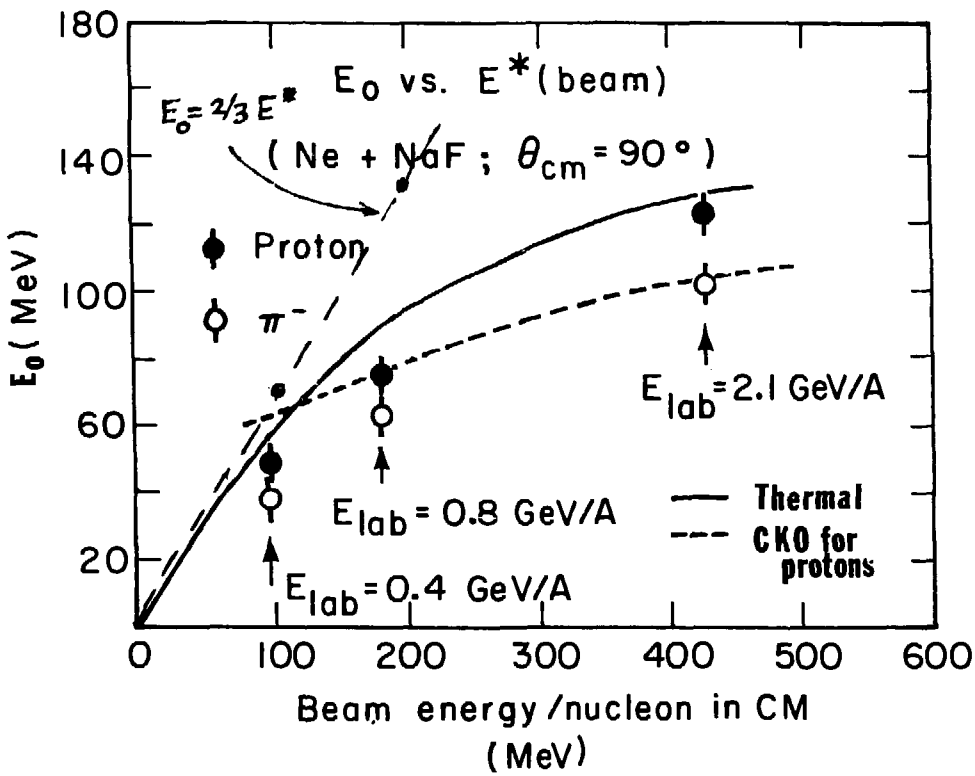

XBL 788-1495A

Fig. 18

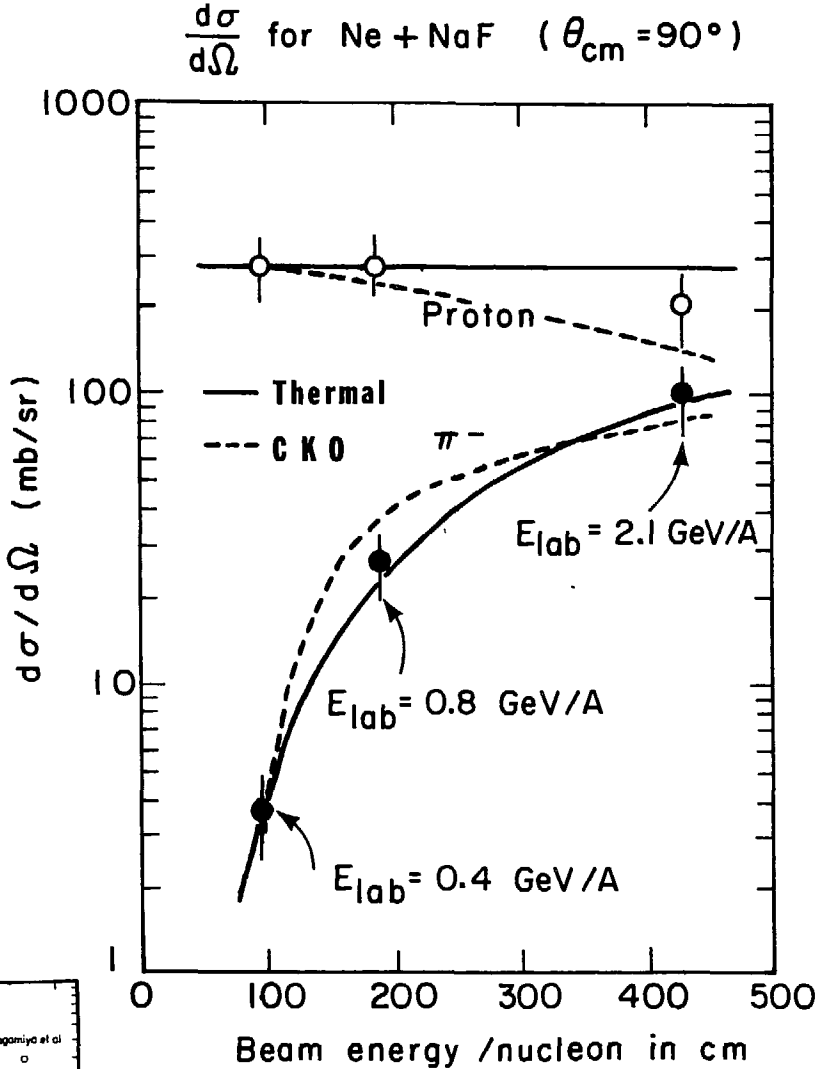

XBL 788-1496A

Fig. 19

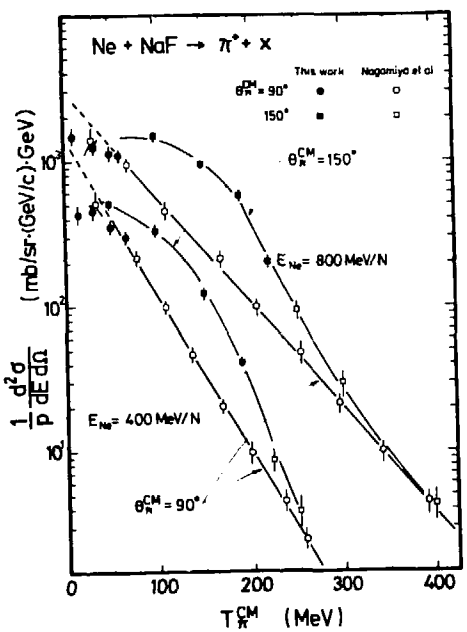

Fig. 20

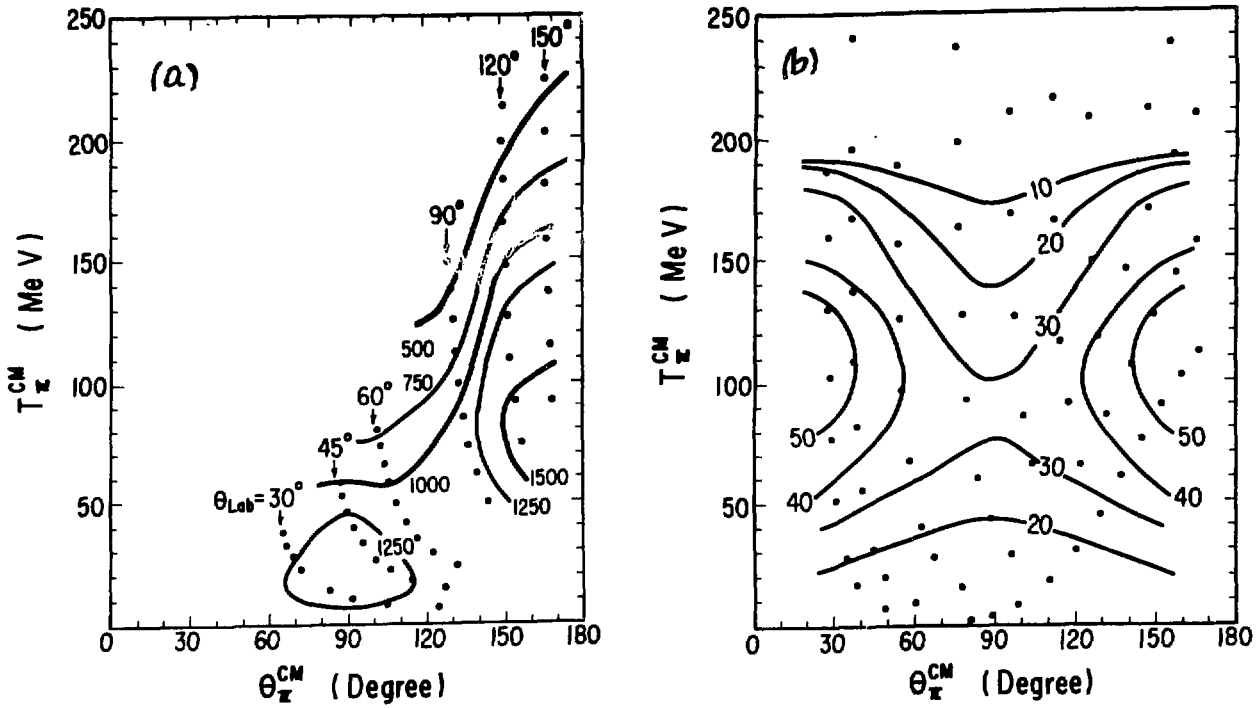
(a)
(b)
250
200
150
100
50
0
30
60
90
120
150
180
T_π^{CM} (MeV)
θ_π^{CM} (Degree)
150°
120°
90°
60°
45°
θ_{Lab}= 30°
500
750
1000
1250
1500
1250
10
20
30
50
40
30
50
40
20

Fir 21

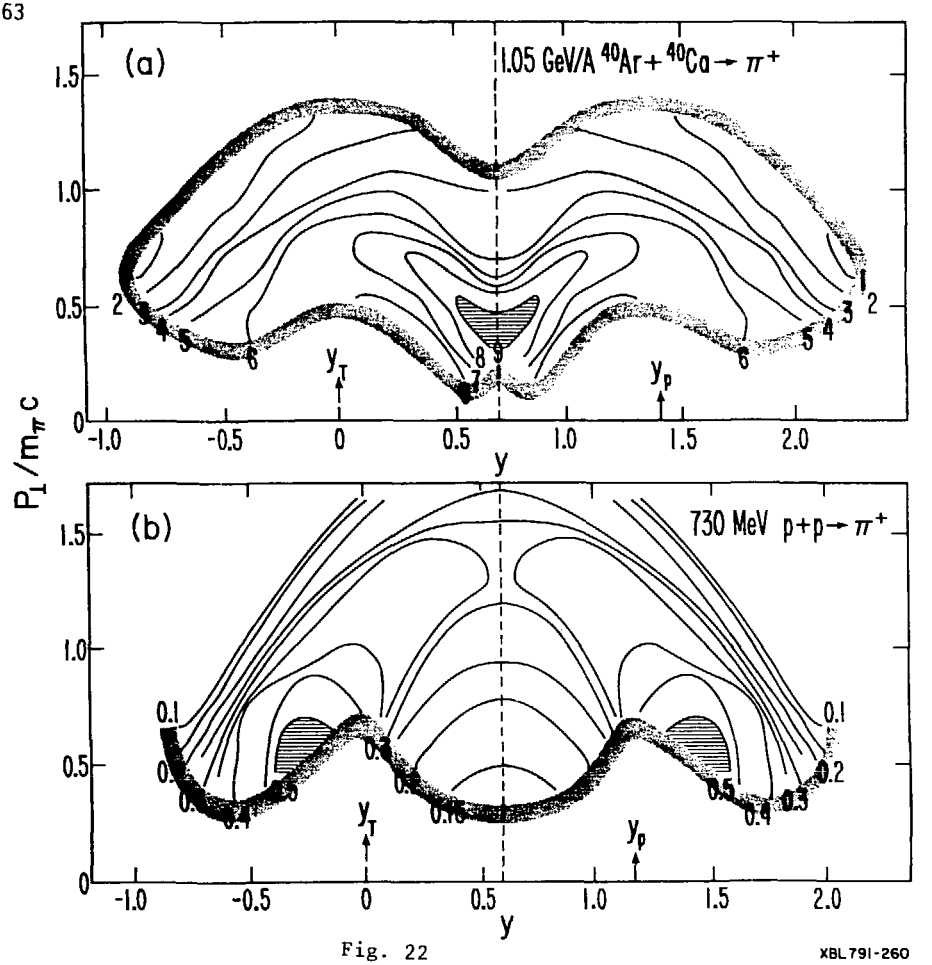
(a)
1.05 GeV/A ^{40}Ar+^{40}Ca→ π^+
(b)
730 MeV p+p→ π^+
$P_\perp/m_\pi c$
y
y_T
y_p
XBL791-260

Fig. 22

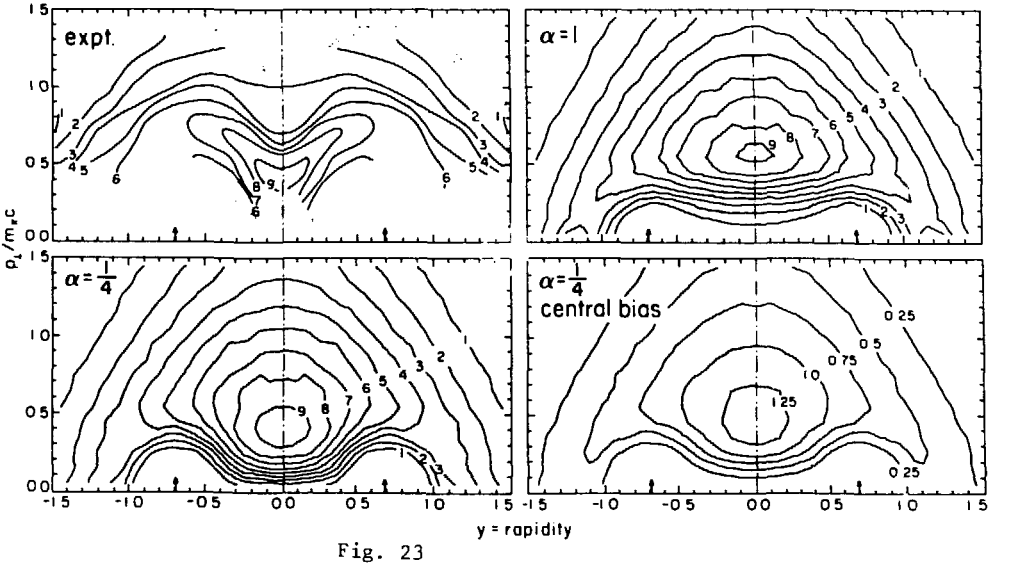
expt.
α=1
α=1/4
α=1/4
central bias
$p_\perp/m_\pi c$
y = rapidity

Fig. 23

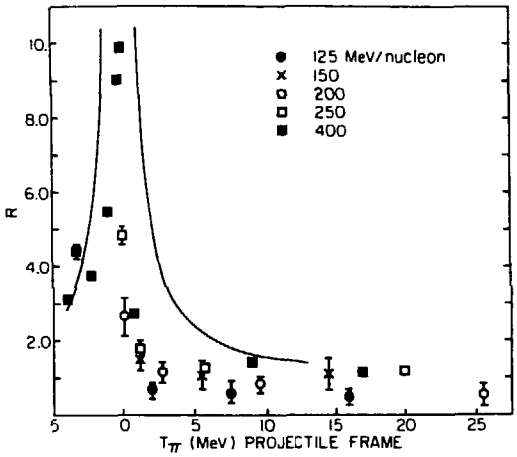
125 MeV/nucleon
150
200
250
400
R
10.
8.0
6.0
4.0
2.0
5
0
5
10
15
20
25
T_π (MeV) PROJECTILE FRAME

Fig. 24

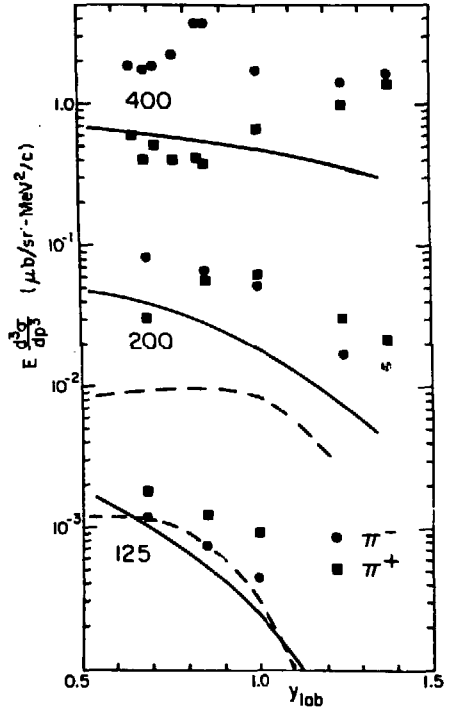
400
200
125
1.0
10^{-1}
10^{-2}
10^{-3}
$E\frac{d^3\sigma}{dp^3}$ (μb/sr-MeV^2/c)
π^-
π^+
0.5
1.0
1.5
y_{lab}

Fig. 25

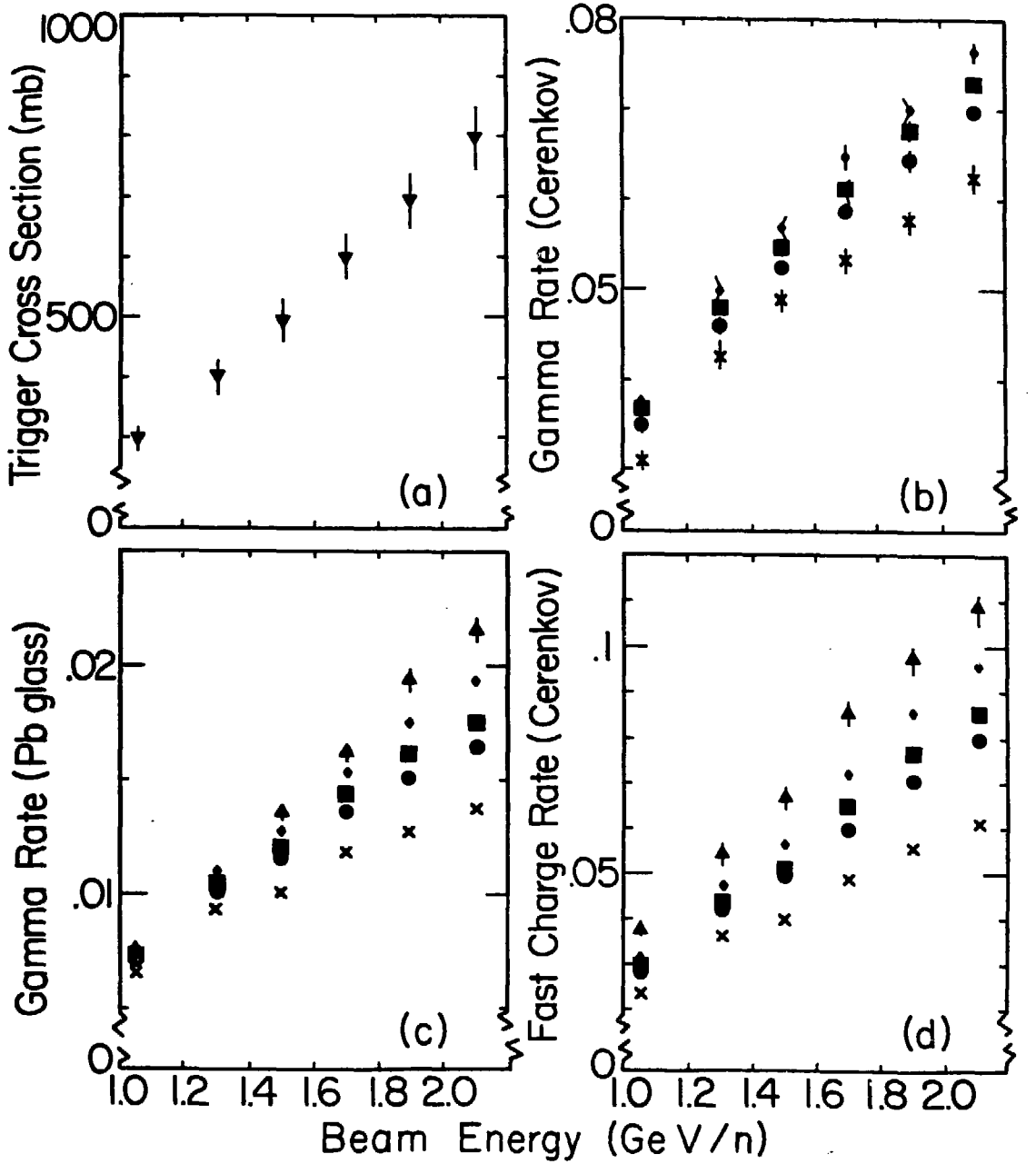
Trigger Cross Section (mb)
1000
500
0
(a)
Gamma Rate (Cerenkov)
.08
.05
0
(b)
Gamma Rate (Pb glass)
.02
.01
0
(c)
Fast Charge Rate (Cerenkov)
.1
.05
0
(d)
1.0 1.2 1.4 1.6 1.8 2.0
Beam Energy (GeV/n)

Fig. 26

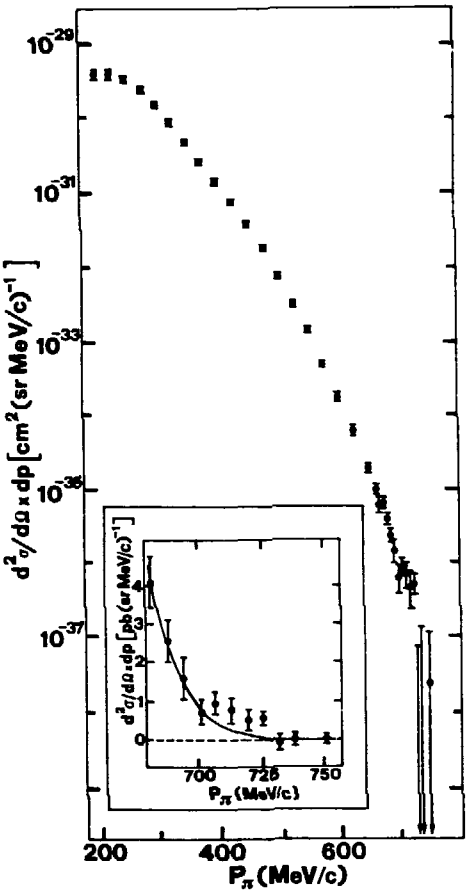

Fig. 27

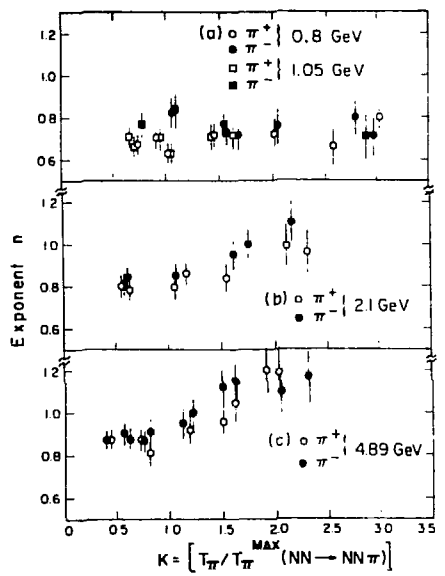

Fig. 29

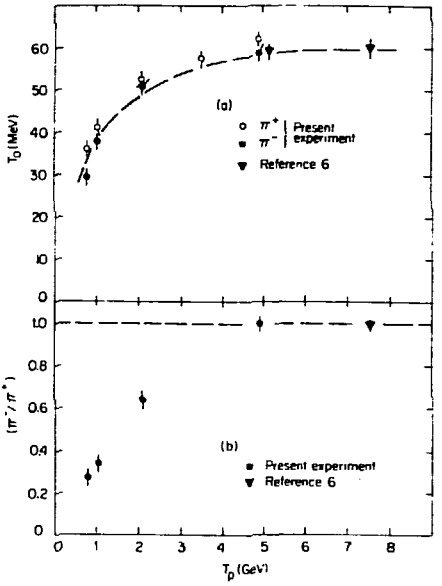

Fig. 28

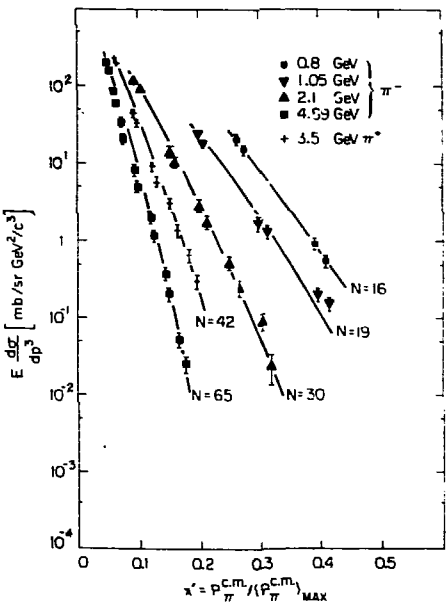

Fig. 30

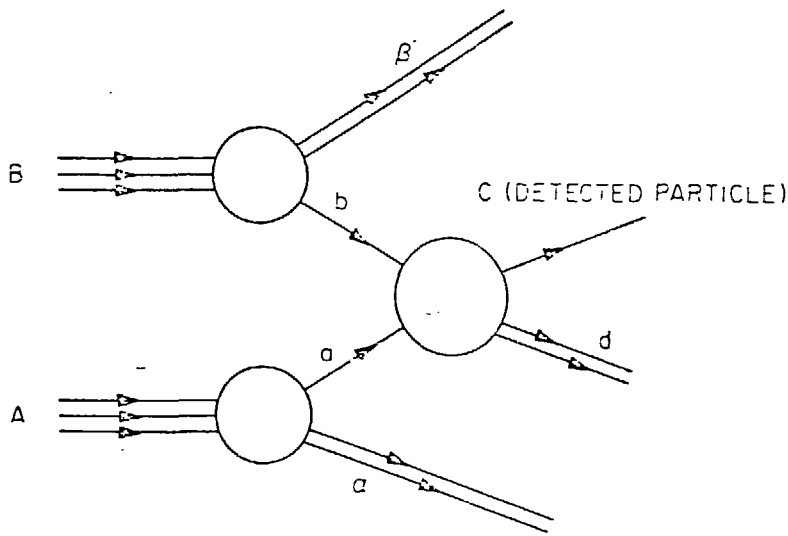

Fig. 31

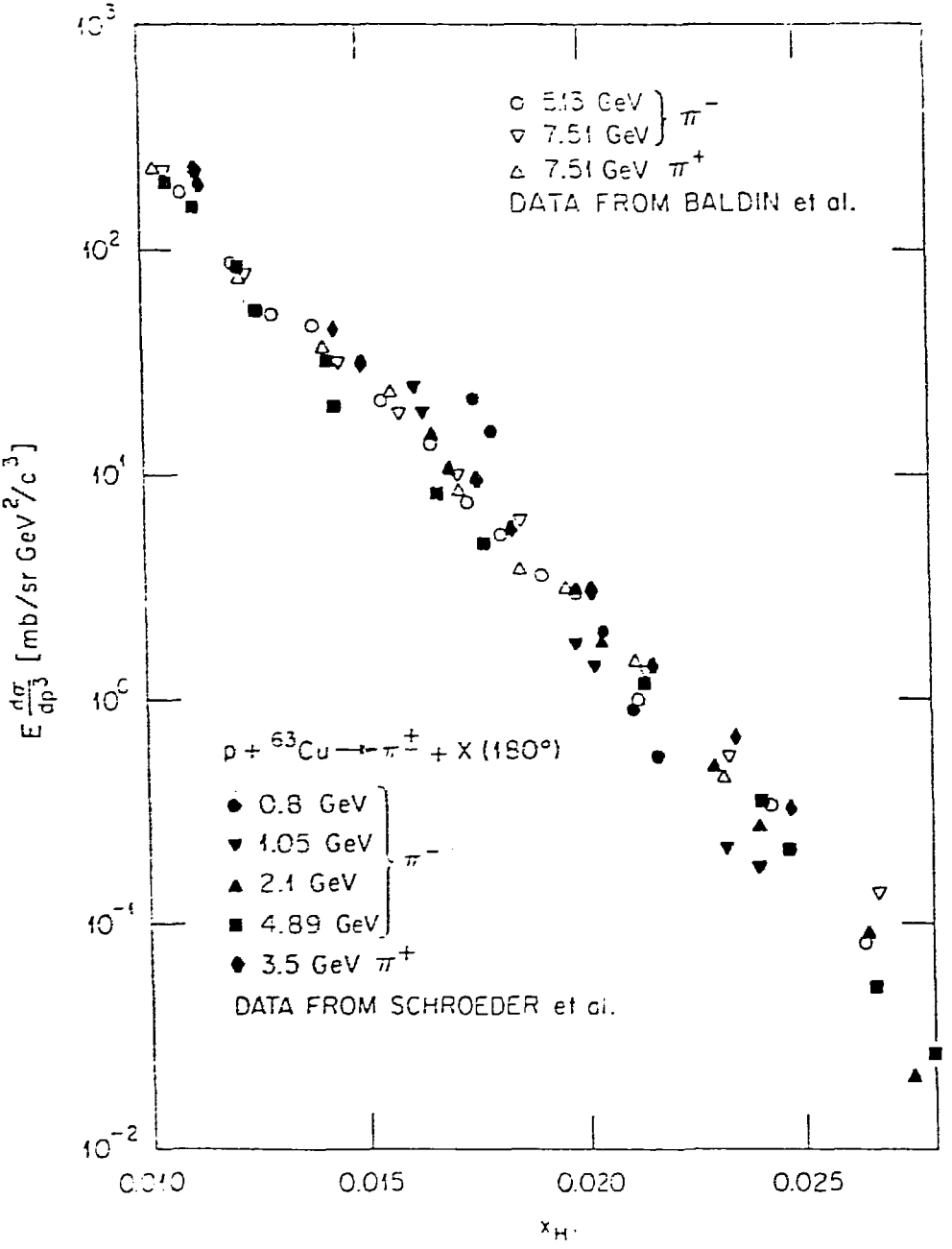
5.13 GeV
7.51 GeV
π⁻
7.51 GeV π⁺
DATA FROM BALDIN et al.
p + ⁶³Cu → π± + X (180°)
0.8 GeV
1.05 GeV
2.1 GeV
4.89 GeV
π⁻
3.5 GeV π⁺
DATA FROM SCHROEDER et al.
E dσ/dp³ [mb/sr GeV²/c³]
x_H
0.010
0.015
0.020
0.025

Fig. 32

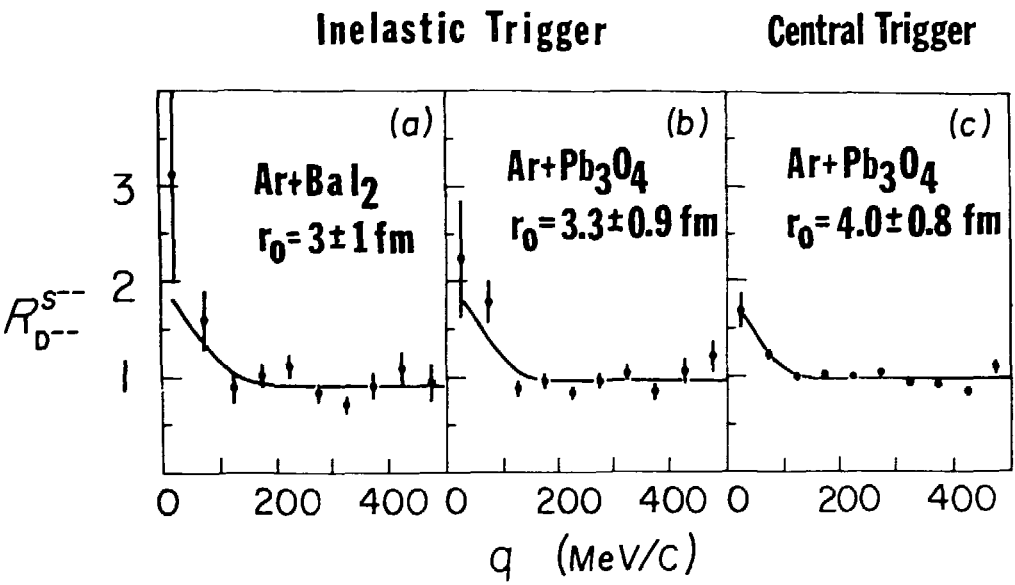
Inelastic Trigger
Central Trigger
(a)
Ar+BaI2
r0=3±1fm
(b)
Ar+Pb3O4
r0=3.3±0.9 fm
(c)
Ar+Pb3O4
r0=4.0±0.8 fm
R s-- D--
3
2
1
0
200
400
q (MeV/c)

Fig. 33

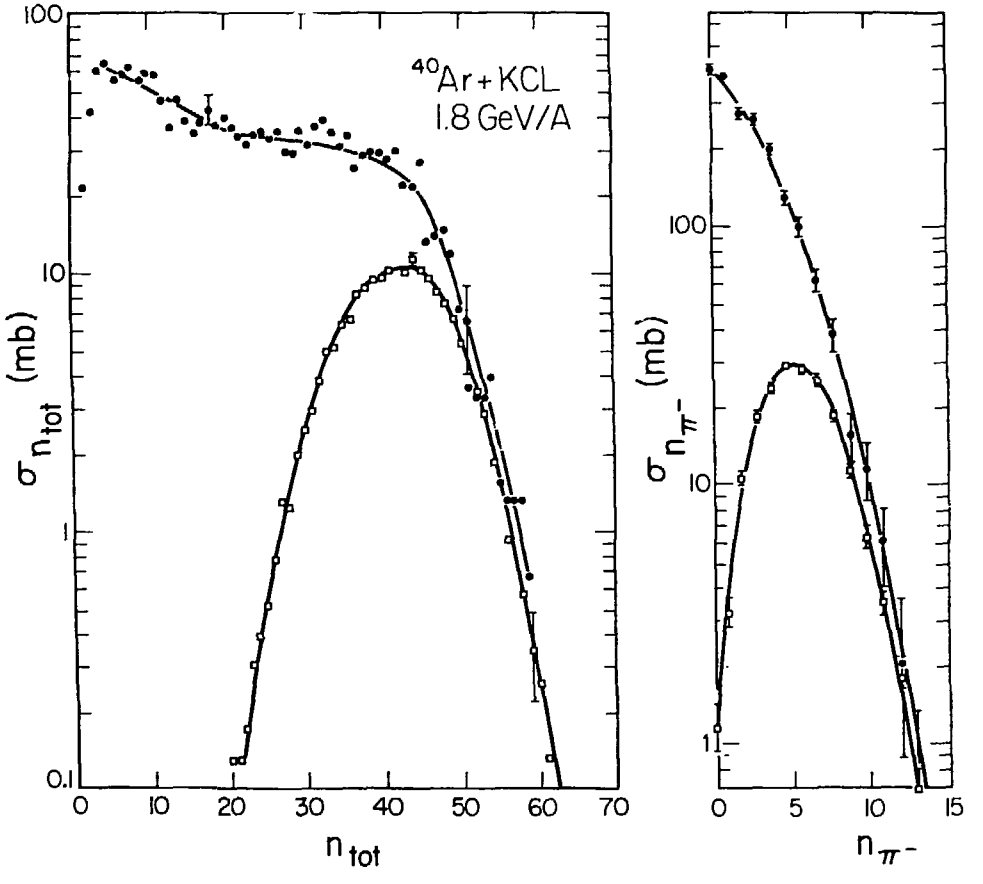
^{40}Ar+KCL
1.8 GeV/A
$\sigma_{n_{tot}}$ (mb)
n_{tot}
$\sigma_{n_{\pi^-}}$ (mb)
n_{π^-}
XBL 804-704

Fig. 34

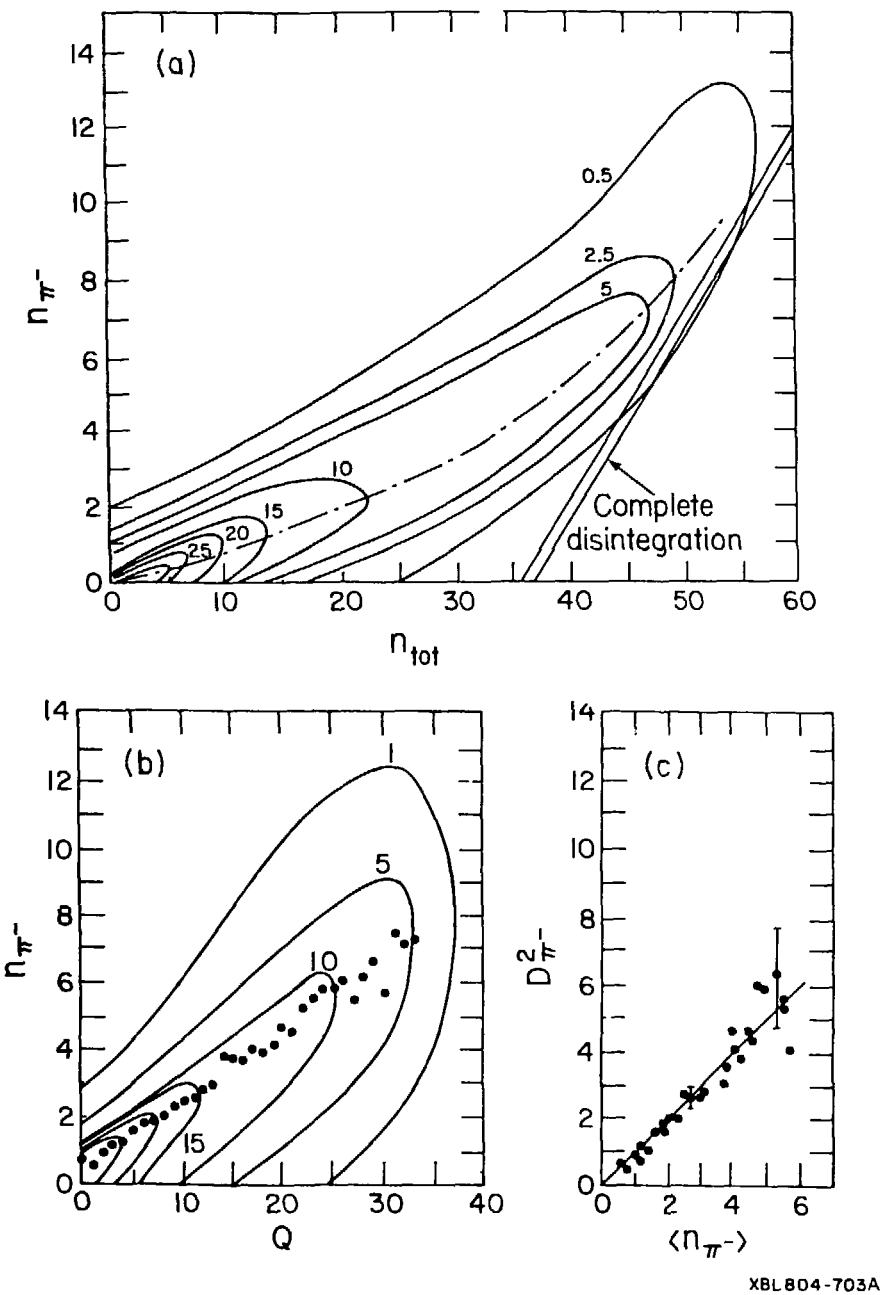
(a)
0.5
2.5
5
10
15
20
25
Complete
disintegration
n_{π^-}
n_{tot}
(b)
1
5
10
15
Q
(c)
$D^2_{\pi^-}$
$\langle n_{\pi^-} \rangle$
XBL804-703A

Fig. 35

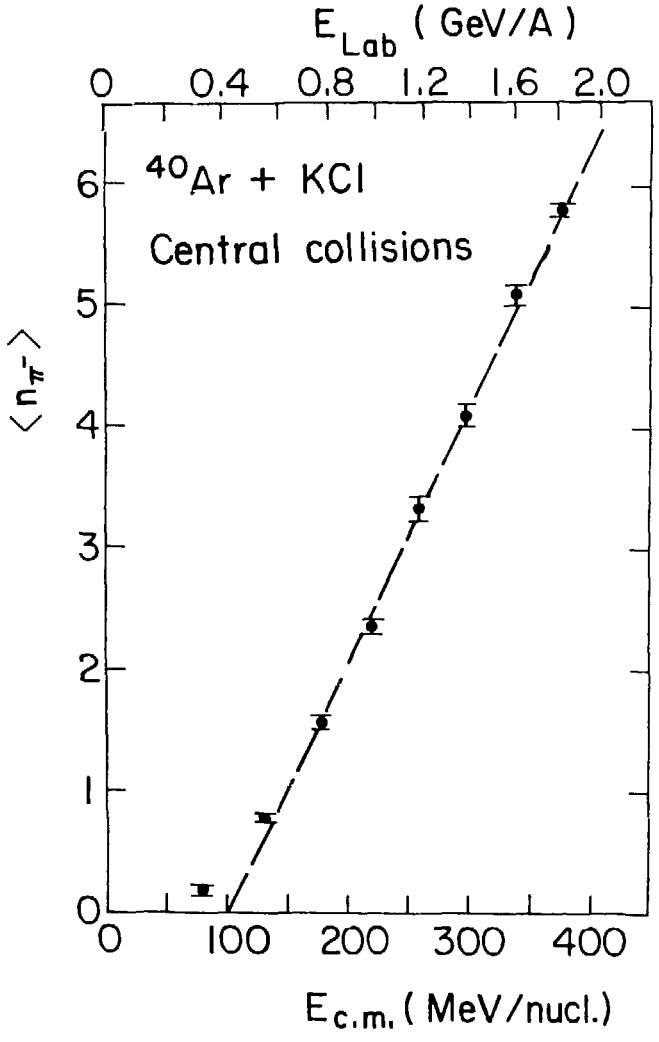

XBL 804 - 701

Fig. 36

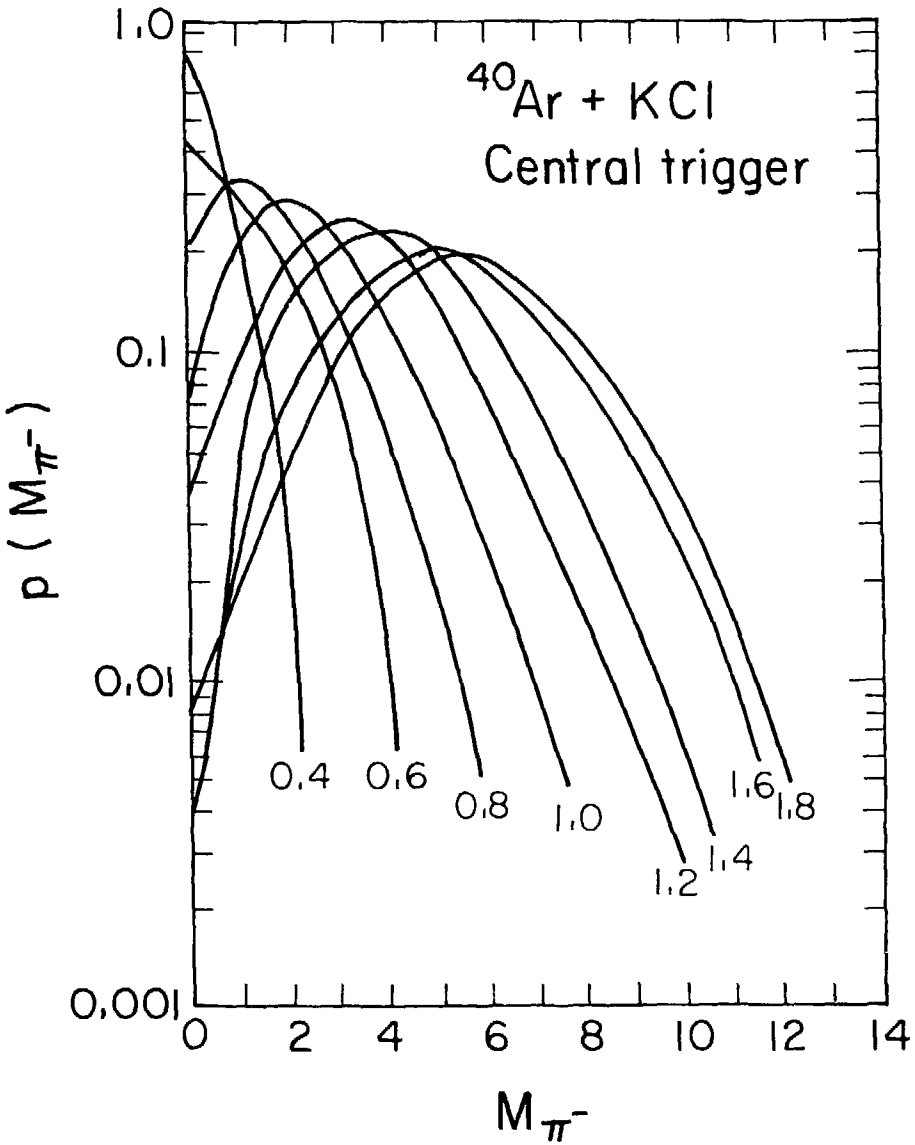
1.0
0.1
0.01
0.001
0
2
4
6
8
10
12
14
^{40}Ar + KCl
Central trigger
p (M_{π^-})
M_{π^-}
0.4
0.6
0.8
1.0
1.2
1.4
1.6
1.8
XBL 804-751

Fig. 37

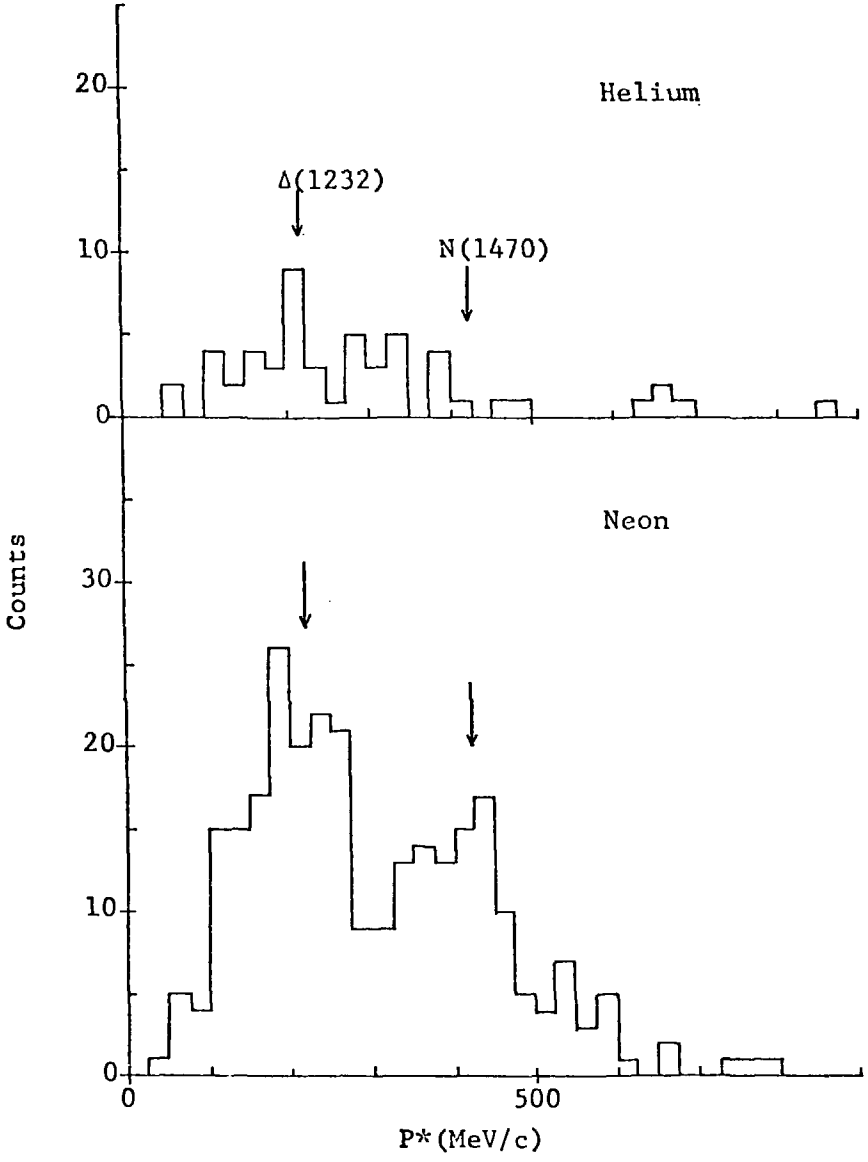

Fig. 38

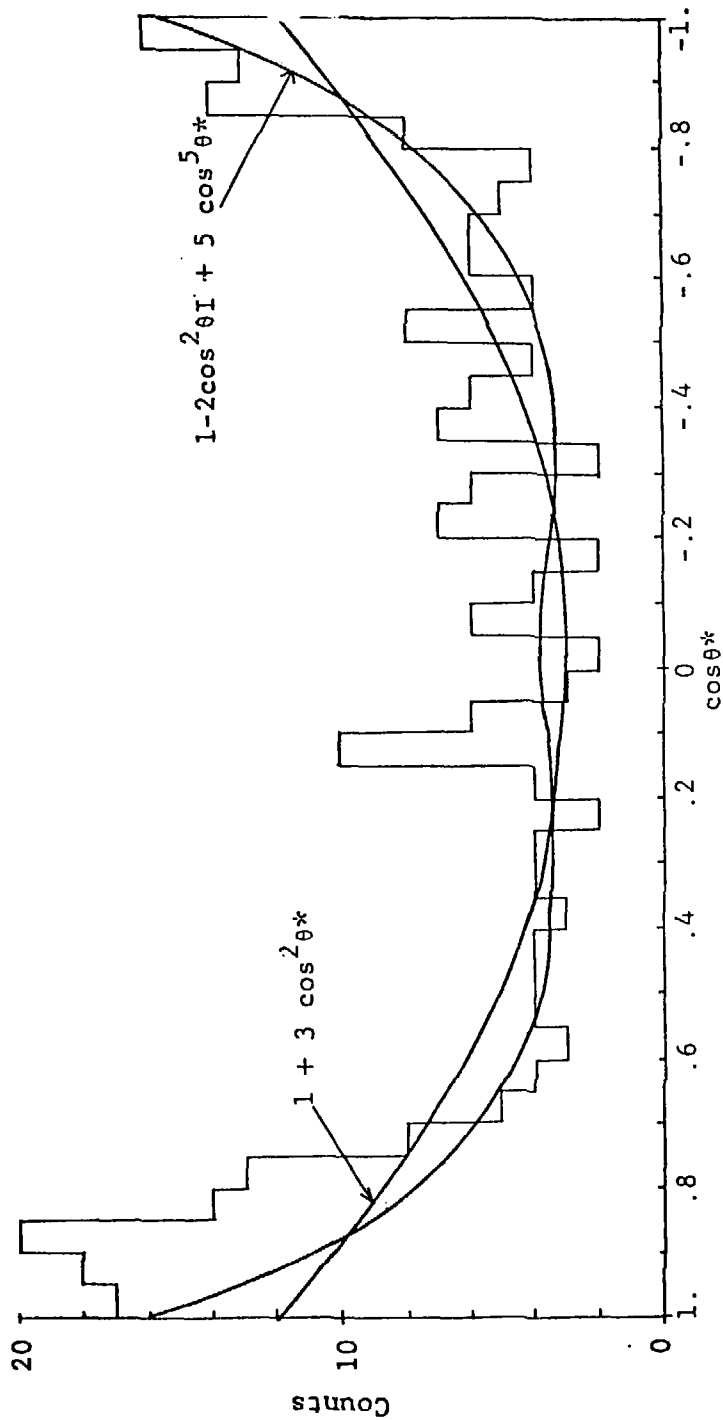

Fig. 39